PROCEEDINGS A

royalsocietypublishing.org/journal/rspa

CC BY

Research

Cite this article: Zhang Y, Lunati I. 2026 Sorption–deformation coupling in soft nanoporous materials: insights from a three-phase poromechanics theory. *Proc. R. Soc. A* **482**: 20251094.
https://doi.org/10.1098/rspa.2025.1094

Received: 16 December 2025
Accepted: 13 March 2026

Subject Areas:
materials science, mechanics, thermodynamics

Keywords:
poromechanics, sorption, nanoporous, disjoining pressure, swelling, large strain

Author for correspondence:
Yida Zhang
e-mail: Yida.Zhang@Colorado.edu

Electronic supplementary material is available online at https://doi.org/10.6084/m9.figshare.c.8407467.

THE ROYAL SOCIETY PUBLISHING

Sorption–deformation coupling in soft nanoporous materials: insights from a three-phase poromechanics theory

Yida Zhang[1] and Ivan Lunati[2]

[1]Department of Civil, Environmental and Architectural Engineering, University of Colorado Boulder, Boulder, CO 80309, USA
[2]Laboratory for Computational Engineering, Swiss Federal Laboratories for Materials Science and Technology, Dübendorf 8600, Switzerland

YZ, 0000-0002-1505-6678

We develop a large-strain poromechanics theory for the coupled sorption–deformation behaviours exhibited by many soft nanoporous materials. Instead of modelling sorption as a molecular mixing process as in classical gel theories, we interpret it as a nanopore-level phenomenon that alters pore-scale interactions and thereby affects the macroscopic response of the porous solid. The proposed theory primarily follows the poromechanics formulation of Coussy (Coussy 2004 *Poromechanics*. Chichester: John Wiley & Sons, Ltd) and its enrichment with surface thermodynamics (Zhang 2018 *J. Mech. Phys. Solids* **114**, 31–54). Specifically, we treat the system as a three-phase mixture by separately listing the balance laws of the solid, the bulk fluid and the sorbed excess phases, which are then combined to deduce the free energy imbalance of the system. Examining individual dissipation terms leads to the general forms of transport laws, reaction kinetics, constitutive relations of the porous solid and the equations of state (EOS) of the bulk and the excess fluids. We demonstrate that, in the presence of sorption, the equivalent pore pressure that drives changes of fluid-accessible porosity is no longer solely the bulk fluid pressure, as assumed in traditional poromechanics theories,

© 2026 The Authors. Published by the Royal Society under the terms of the Creative Commons Attribution License http://creativecommons.org/licenses/by/4.0/, which permits unrestricted use, provided the original author and source are credited.

Downloaded from http://royalsocietypublishing.org/rspa/article-pdf/doi/10.1098/rspa.2025.1094/6136174/rspa.2025.1094.pdf
by guest
on 07 May 2026

but includes an additional disjoining pressure arising from the sorbed excess. We confirm that the disjoining pressure isotherm and the sorption isotherm are fundamentally the two sides of the same coin, both characterized by the free energy potential of the excess phase. A simple four-parameter model for amorphous cellulose (AC) interacting with water vapour is constructed using only elementary, textbook-level constitutive laws for the individual phases. Despite its simplicity, the model exhibits remarkable predictive capability in capturing the complex, nonlinear sorption–deformation coupling of the material. Finally, we show that the chemomechanical formulation of Gurtin *et al.* (Gurtin *et al.* 2010 *The mechanics and thermodynamics of continua*. Cambridge University Press) and the gel theory of Hong *et al.* (Hong *et al.* 2008 *J. Mech. Phys. Solids* **56**, 1779–1793) can be retrieved by reducing the 'resolution' of the proposed theory through eliminating the porosity terms and combining the bulk fluid and the sorbed excess phases. The modularity and versatility of the proposed theory make it well-suited for applications beyond polymeric materials, extending to a broad class of nanoporous systems with diverse microstructures and physicochemical interactions with surrounding fluids.

1. Introduction

Soft nanoporous materials having characteristic pore sizes below 100 nm are ubiquitous in nature (e.g. tissue scaffold, cellulose, clay) and in engineering applications (e.g. foams, gels, metal-organic frameworks). These materials often exhibit significant swelling/shrinkage upon sorption/desorption of fluids owing to nanoconfinement effects resulted from their network topology and interfacial interactions [1,2]. Nature uses such stimuli-responsive features of cellulose nanofibres to facilitate the dispersal of plant seeds upon humidity change [3]. Bioinspired nanoporous networks based on polymers have been recently developed for fast and reliable actuators [4–6], gas sensors [7] and artificial muscles [8] driven by sorption of solvent molecules. To enhance predictions and enable design-driven control of hygroscopic or sorption-driven movements, it is essential to advance our fundamental understanding and develop robust continuum theories that capture the coupling between sorption and deformation in soft nanoporous materials.

Several continuum theories exist for modelling such systems. One of the foundational works is the chemomechanical framework of Gurtin *et al.* [9]. By introducing chemical potential μ as a primitive quantity characterizing the energy exchanges owing to species transport, the free energy imbalance of an open material representative elementary volume (REV) can be written in Lagrangian form as [9]

$$\mathbf{S} : \dot{\mathbf{E}} + \mu \dot{N} - \mathbf{H} \cdot \nabla_{\mathbf{X}} \mu - \dot{\Psi} = \Lambda \geq 0, \tag{1.1}$$

where $\mathbf{S}$ is the Second Piola–Kirchhoff stress and $\mathbf{E}$ is the Green–Lagrangian strain (defined later after equation (2.4)); N is the number of diffusing species per reference volume of the REV; μ is the chemical potential by mole; $\mathbf{H}$ is the Lagrangian species flux vector; Ψ is the Helmholtz free energy of the REV; Λ is the rate of dissipation. The transport laws and the constitutive equations can be subsequently established through the Coleman–Noll procedure [10]. In this vein, we may group all models that focus on coupling the overall kinematics of the REV (e.g. deformation gradient $\mathbf{F}$) and the chemical variables of the invading fluid molecules (e.g. concentration N or chemical potential μ) as chemomechanical models. Hong *et al.* [11] proposed a chemomechanical theory for gels, where the sorption-induced swelling is modelled through a mixing contribution Ψ_{mix} [12] in the total Helmholtz free energy of the REV:

$$\Psi(\mathbf{F}, N) = \Psi_{\text{stretch}}(\mathbf{F}) + \Psi_{\text{mix}}(N), \tag{1.2}$$

where Ψ_{stretch} captures the usual hyperelastic behaviour of the polymer network. Brochard *et al.* [13] proposed a small-strain chemoelasticity theory for modelling coal swelling during

Downloaded from http://royalsocietypublishing.org/rspa/article-pdf/doi/10.1098/rspa.2025.1094/6136174/rspa.2025.1094.pdf
by guest
on 07 May 2026

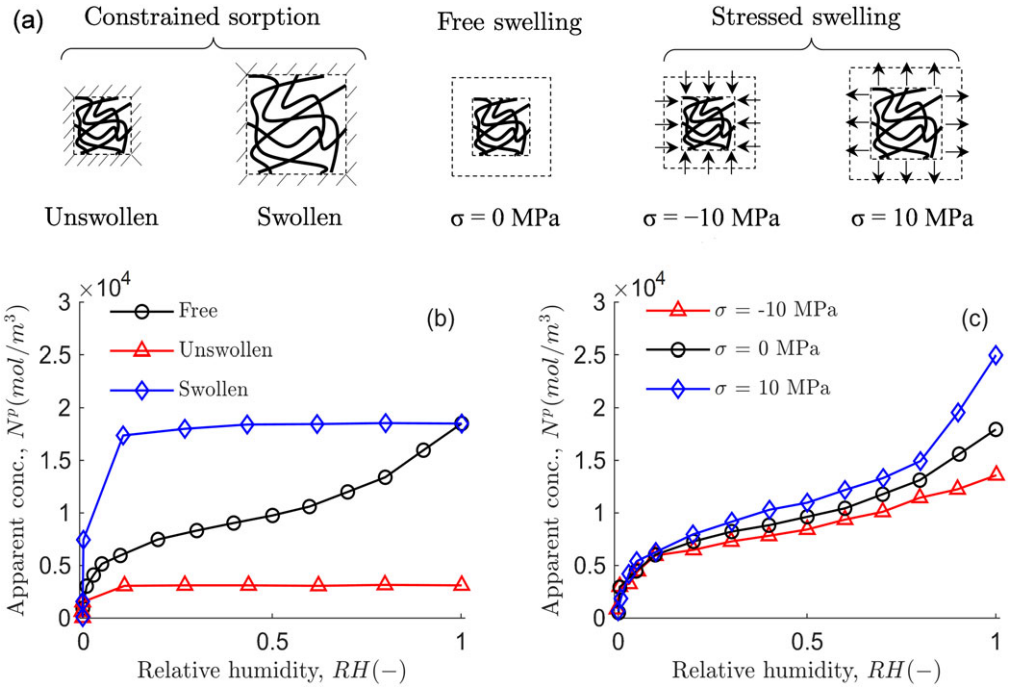

Figure 1. Interaction between amorphous cellulose (AC) and water vapour: (a) schematic of different types of sorption tests; (b) sorption isotherms from strain-controlled tests; (c) sorption isotherms from stress-controlled tests; N^p is the apparent concentration, defined as the number of moles of pore fluid per unit reference volume of the material; σ is the isotropic stress applied to the material. Data from molecular dynamics (MDs) simulations are reported in Chen *et al.* [2].

methane sorption. The mechanical consequence of sorption is introduced by considering a strain-dependent sorption isotherm $N(\varepsilon, \mu)$, combined with equation (1.1) and assuming a linear elastic solid:

$$\sigma = K\varepsilon - \frac{\partial}{\partial \varepsilon}\left[\int_{-\infty}^{\mu} N(\varepsilon, \mu)\mathrm{d}\mu\right], \tag{1.3}$$

where σ is the mean Cauchy stress and ε is the volumetric infinitesimal strain, respectively; K is the bulk modulus. A simpler version of equation (1.3) is to replace the last term by a linear term $\alpha K \Delta\mu$ or alike. For water-induced swelling, the coefficient α is referred to as the *hygrometric expansion coefficient*, analogous to the thermal expansion coefficient in thermoelasticity [6,14,15].

Although chemomechanical models successfully capture the overall phenomenology of sorption-induced swelling, the lack of microstructural descriptors makes them less straightforward for describing the inherently two-way, nonlinear and often hysteretic nature of sorption–deformation coupling. Indeed, the apparent sorption isotherm of soft nanoporous materials depends strongly on its deformation (figure 1a). For example, amorphous cellulose (AC) exhibits a markedly greater capacity to capture and retain water molecules when it is initially expanded to a swollen state than when it is initially constrained at an unswollen state (figure 1b). Similarly, under stress-controlled conditions, the imposition of an isotropic compressive stress suppresses sorptive uptake relative to free-swelling or tensile-stressed conditions (figure 1c).

In this regard, poromechanics theory offers distinct advantages by capturing solid–fluid coupling through the explicit incorporation of microstructural features of these materials [16]. Specifically, by treating porosity ϕ and deformation gradient $\mathbf{F}$ as two independent kinematic variables, one can account for the compressibility of the solid constituents for more general material systems and loading conditions. Coussy *et al.* [17] demonstrated that Biot's theory for saturated porous media can be derived from the mixture theory of multiphase, multicomponent

Downloaded from http://royalsocietypublishing.org/rspa/article-pdf/doi/10.1098/rspa.2025.1094/6136174/rspa.2025.1094.pdf
by guest
on 07 May 2026

systems [18,19], thus providing a rigorous thermodynamic foundation for poromechanics. Attempts have been made to extend the Biot–Coussy's framework for modelling sorption-driven swelling by introducing surface energy in the system's total free energy expression, thereby translating environmental effects on surface energy into the macroscopic responses of porous materials [20–22]. The actions of surface stresses and capillary forces in nanopores have also been shown mathematically to influence the overall deformation of the solid matrix [23–25]. Along these lines, *surface poromechanics* (SP) [26], derived from first principles within mixture theory, provides a comprehensive thermodynamic treatment of interfaces in porous materials. In SP, the solid–fluid interface (or the pore wall) is viewed as an independent phase that can carry its own mass, momentum and energy. As a result, the specific surface area appears in the free energy imbalance equation, thereby enhancing the description of material microstructure in addition to porosity. This enrichment permits the continuum description of porous materials to capture not only tangential interfacial interactions such as surface stress [26], but also normal interactions such as disjoining pressure and other surface forces [27]. The SP approach straightforwardly handles compressible solid and fluid constituents, and it is readily extendable to arbitrary pore size distributions [28] and heterogeneous pore fluids [29]. SP models have been successfully applied to predict permeability evolution during coalbed methane extraction [30] and the hygromorphs of sorptive bilayers during humidity changes [31].

One obstacle to applying SP to nanoporous materials lies in the mismatch in microstructural representation. As correctly pointed out by Chen *et al.* [2] and Brochard *et al.* [13], for nanoporous materials like AC, sorption can no longer be described by surface covering as conceptualized in SP. Identifying a solid–fluid surface area for polymer networks is challenging, although the concept of porosity or pore size can still be nominally defined by examining fluid-accessible volumes. This challenge extends to most nanoporous materials, where the phase boundary between solid and fluid becomes ambiguous over several molecular lengths. In this context, the objectives of this work are twofold: (1) to establish a general thermodynamic framework for nanoporous materials interacting with sorptive species that avoids reliance on the concept of surface area and (2) to develop a large-strain constitutive model within this framework and evaluate its capability in predicting the full sorption–deformation coupling of AC. The paper is structured as follows: §2 revisits the balance laws of the mixture, which included a novel volume-averaged (rather than surface-averaged) excess phase. In §3, we explore the implications of the free energy imbalances and derive the general-form conduction laws, reaction kinetics and constitutive relations for individual phases. In §4, we demonstrate the application of the theory by introducing a simple, effective stress-based constitutive model for AC interacting with water vapour. The model's performance in predicting the two-way coupling between sorption and deformation is evaluated against existing molecular simulation datasets. In §5, we discuss alternative forms of constitutive laws, highlight the uniqueness of the Coussy procedure and demonstrate the consistency of the proposed framework with previous theories. Finally, in §6, we provide concluding remarks and outline future prospects.

2. Nanoporous material as a three-phase mixture

(a) Conceptualizations and notations

The system under consideration is a nanoporous polymer infiltrated by fluid species through its interstitial or 'pore' spaces, as shown in figure 2. A similar idealization can be drawn for generic nanoporous materials.

One of the main novelties of the present work, distinguishing it from prior chemomechanics, gel mechanics and poromechanics theories, lies in its conceptual treatment of the pore fluid. In nanopores, fluids occupying these tight spaces experience pronounced confinement effects from solid–fluid interactions and are therefore often described as *nanoconfined fluids* [32]. Their physical properties are drastically different from their bulk counterparts, with notably higher density and viscosity and the emergence of anisotropic structure [33,34]. To handle this deviation from the

Downloaded from http://royalsocietypublishing.org/rspa/article-pdf/doi/10.1098/rspa.2025.1094/6136174/rspa.2025.1094.pdf
by guest
on 07 May 2026

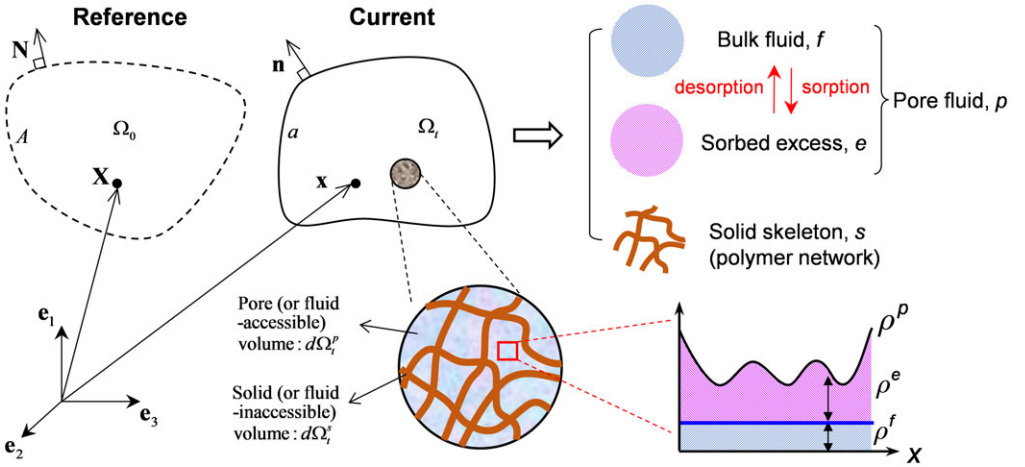

Figure 2. System under consideration: a nanoporous material idealized as a mixture of solid, bulk fluid and sorbed excess phases.

usual bulk fluid properties, we propose to treat the nanoconfined pore fluid as a superposition of a bulk (free) fluid phase that one would find in a remote reservoir and a *sorbed excess phase*, both of which occupy the same pore space. This treatment shares the same spirit as the celebrated Gibbs surface excess approach [35,36], in which the extra fluid mass near a solid surface owing to solid–fluid interaction is lumped into a *surface excess* phase, thereby greatly simplifying the analysis of a sorption phenomenon [37]. Indeed, in the Gibbs framework, the familiar notion of surface energy emerges as the excess free energy of the interface per unit area relative to the two neighbouring bulk phases. Our treatment here differs from Gibbs's in that the sorbed excess is volumetrically distributed throughout the entire pore, coexisting with the bulk fluid, instead of being concentrated on an ideal, zero-thickness surface. This is justified by experimental and numerical observations that interfaces occupy a finite thickness rather than a mathematical surface, a feature that becomes pronounced when neighbouring pore walls are separated by only a few molecular diameters [38,39]. Such treatment also effectively eliminates the need to specify a solid–fluid interface area and thereby circumvents the ambiguities associated with defining phase boundaries at nanometre scales [13]. For the same reason, we have chosen a more general term 'sorption' to denote fluid uptake, rather than 'adsorption' or 'absorption', since distinguishing them is often challenging in nanoporous materials [40].

The system is therefore modelled as a mixture of three phases: the solid phase, the bulk fluid phase and the sorbed excess phase denoted by superscripts s, f and e, respectively (figure 2). The solid skeleton is open, deformable and active (i.e. sorptive). Considering a motion $\mathbf{x} = \mathbf{x}(\mathbf{X}, t)$ where $\mathbf{x}$ is the spatial position and $\mathbf{X}$ is the position of the solid particle at time $t = 0$, an arbitrary line segment $\mathrm{d}\mathbf{x}$ and volume element $\mathrm{d}\Omega_t$ can be mapped from the reference configuration $\mathrm{d}\mathbf{X}$ and $\mathrm{d}\Omega_0$ via $\mathrm{d}\mathbf{x} = \mathbf{F} \cdot \mathrm{d}\mathbf{X}$ and $\mathrm{d}\Omega_t = J\mathrm{d}\Omega_0$, where $\mathbf{F} = \nabla_X \mathbf{x}$ is the deformation gradient; $J = \det \mathbf{F} = \mathrm{d}\Omega_t / \mathrm{d}\Omega_0$ is the Jacobian or the volume ratio; ∇_X denotes gradient with respect to material coordinate $\mathbf{X}$. The velocity of the solid skeleton is $\mathbf{v}^s(\mathbf{x}, t)$.

Owing to the porous nature of the solid, the volume element $\mathrm{d}\Omega_t$ can be decomposed into pore volume $\mathrm{d}\Omega_t^p$ and solid volume $\mathrm{d}\Omega_t^s$ that satisfies $\mathrm{d}\Omega_t = \mathrm{d}\Omega_t^p + \mathrm{d}\Omega_t^s$. For nanoporous materials, it is useful to generalize the concept of pore as 'fluid-accessible space' that allows the permeation or storage of fluid molecules, and solid volume as 'fluid-inaccessible space' taken up by the solid molecules together with the narrow gaps, corners and disconnected pores formed by their structural arrangement. The smeared solid phase therefore can be compressible although its molecules may be incompressible. The definitions of Eulerian porosity n and Lagrangian porosity ϕ naturally follow $\mathrm{d}\Omega_t^p = n\mathrm{d}\Omega_t = \phi\mathrm{d}\Omega_0$. It is straightforward to show $\phi = Jn$ and $\mathrm{d}\Omega_t^s = (1 - n)\mathrm{d}\Omega_t = (J - \phi)\mathrm{d}\Omega_0$.

Downloaded from http://royalsocietypublishing.org/rspa/article-pdf/doi/10.1098/rspa.2025.1094/6136174/rspa.2025.1094.pdf
by guest
on 07 May 2026

The bulk fluid and excess phases are considered homogeneous and move with absolute velocities $\mathbf{v}^f(\mathbf{x}, t)$ and $\mathbf{v}^e(\mathbf{x}, t)$, respectively. For generality, we further allow the two phases to each consist of k species and that they can differ in composition:

$$\mathcal{N}_i = \mathcal{N}_i^f + \mathcal{N}_i^e; \quad d\mathcal{N}_i^\alpha = n_i^\alpha d\Omega_t = N_i^\alpha d\Omega_0, \tag{2.1}$$

where $\mathcal{N}_i$ is the total number of moles of species i in domain Ω_t; n_i^α and $N_i^\alpha = Jn_i^\alpha$ are, respectively, the number of moles of species i in $\alpha = f, e$ phases per unit current volume $\mathrm{d}\Omega_t$ and reference volume $\mathrm{d}\Omega_0$, also referred to as the *apparent concentration*. Each species may move at a velocity $\mathbf{v}_i^\alpha(\mathbf{x}, t)$ distinct from its corresponding overall phase velocity. The particle derivative of a field with respect to phase α is defined as $d^\alpha(\cdot)/dt = \partial(\cdot)/\partial t + \mathbf{v}^\alpha \cdot \nabla_x(\cdot)$. Given the significantly reduced mobility of sorbed fluid molecules [41], in this paper, we simplify our derivations assuming the excess phase moves synchronously with the solid skeleton (i.e. $\mathbf{v}_i^e = \mathbf{v}^e = \mathbf{v}^s$).

Letters in the calligraphic font denote extensive quantities (e.g. $\mathcal{E}$); upper/lower case letters denote volume-related quantities in reference/current configurations (e.g. E and e), respectively; letters with hat denote mass-related quantities (e.g. $\hat{e}$).

(b) Balance laws

The balance laws for the three-phase (s, f, e) and multicomponent (k species) mixture are derived following the same procedure outlined in Zhang [26] and Coussy [42], and the full details are provided in the electronic supplementary material, §A. The strategy is to first separately list the balanced laws of individual phases with the observing window fixed to the solid skeleton, then combine them to obtain the balance laws of the entire REV. For brevity, only the essential equations are summarized below.

The mass and mole balances and the resulting averaging relations can be found in the electronic supplementary material. The momentum balance of the overall mixture is derived as

$$\nabla_x \cdot \boldsymbol{\sigma} + [\rho^s(1-n) + \rho^e n](\mathbf{f} - \mathbf{a}^s) + \rho^f n(\mathbf{f} - \mathbf{a}^f) = 0, \tag{2.2}$$

where $\boldsymbol{\sigma}$ is the Cauchy stress tensor; $\mathbf{f}$ is the body force; $\mathbf{a}^\alpha = \mathrm{d}^\alpha \mathbf{v}^\alpha / \mathrm{d}t$ is the acceleration vector; superscripts $\alpha = s, f, e$ denote properties of the solid, fluid and excess phases, respectively; ρ^α is the intrinsic density. Comparing to the momentum balance of non-reactive porous media (eqn. (2.19) in Coussy [42]), equation (2.2) has an additional term $\rho^e n(\mathbf{f} - \mathbf{a}^s)$ to account for the inertia and body force carried by the sorbed excess mass.

The internal energy balance of the mixture in Eulerian and Lagrangian forms is derived as

$$\frac{d^s e}{dt} + e\nabla_x \cdot \mathbf{v}^s = \boldsymbol{\sigma} : \nabla_x \mathbf{v}^s + (\mathbf{f} - \mathbf{a}^f) \cdot \hat{\mathbf{w}} - \nabla_x \cdot \left(\hat{h}^f \hat{\mathbf{w}} + \sum \hat{\mu}_i^f \hat{\mathbf{h}}_i\right) - \nabla_x \cdot \mathbf{q} \tag{2.3}$$

and

$$\frac{\partial E}{\partial t} = \mathbf{S} : \frac{\partial \mathbf{E}}{\partial t} + (\mathbf{f} - \mathbf{a}^f) \cdot \mathbf{F} \cdot \hat{\mathbf{W}} - \nabla_X \cdot \left(\hat{h}^f \hat{\mathbf{W}} + \sum \hat{\mu}_i^f \hat{\mathbf{H}}_i\right) - \nabla_X \cdot \mathbf{Q}, \tag{2.4}$$

where $\sum(\cdot)$ stands for $\sum_{i=1}^k (\cdot)$ if not specified otherwise; $\mathbf{S} = \mathbf{F}^{-1} \cdot J\boldsymbol{\sigma} \cdot {}^T\mathbf{F}^{-1}$ the second Piola–Kirchhoff stress; left superscript T means transpose; $\mathbf{E} = (\nabla_X \mathbf{u}^s + {}^T\nabla_X \mathbf{u}^s + {}^T\nabla_X \mathbf{u}^s \cdot \nabla_X \mathbf{u}^s)/2$ is the Green–Lagrangian strain with $\mathbf{u}^s = \mathbf{x} - \mathbf{X}$ being the displacement vector; $\mathbf{q}$ and $\mathbf{Q} = J\mathbf{F}^{-1} \cdot \mathbf{q}$ denote the Eulerian and Lagrangian heat flux vectors, respectively, related by the Piola transformation [43]; $\hat{\mathbf{w}} = \rho^f n(\mathbf{v}^f - \mathbf{v}^s)$ and $\hat{\mathbf{W}} = J\mathbf{F}^{-1} \cdot \hat{\mathbf{w}}$ are the Eulerian and Lagrangian fluid–solid relative flow vectors by mass, respectively; $\hat{\mathbf{h}}_i = M_i n_i^f (\mathbf{v}_i^f - \mathbf{v}^f)$ and $\hat{\mathbf{H}}_i = J\mathbf{F}^{-1} \cdot \hat{\mathbf{h}}_i$ are the Eulerian and Lagrangian species–fluid relative flow vectors by mass, respectively; M_i is the molar mass of species i; $e = \rho^s(1-n)\hat{e}^s + \rho^f n\hat{e}^f + \rho^e n\hat{e}^e$ and $E = Je$ are the overall internal energy per current and reference volume, respectively; $\hat{e}^\alpha$ is the mass-specific internal energy; $\hat{\mu}_i^\alpha$ is the mass-specific chemical potentials of species i in the $\alpha = f, e$ phases; $\hat{h}^f$ is the mass-specific enthalpy of the bulk fluid. It is helpful to recall that, for a homogeneous multicomponent fluid, the internal

Downloaded from http://royalsocietypublishing.org/rspa/article-pdf/doi/10.1098/rspa.2025.1094/6136174/rspa.2025.1094.pdf
by guest
on 07 May 2026

energy $\hat{e}^f$, enthalpy $\hat{h}^f$, Helmholtz free energy $\hat{\psi}^f$ and Gibbs free energy $\hat{g}^f$ are interrelated through [26]

$$\begin{aligned}
\hat{h}^f(p,\hat{s}^f,\hat{X}^f_1,\ldots,\hat{X}^f_k) &\equiv \hat{e}^f + \frac{p}{\rho^f} = T\hat{s}^f + \sum \hat{\mu}^f_i \hat{X}^f_i,\\
\hat{\psi}^f\left(\frac{1}{\rho^f},T,\hat{X}^f_1,\ldots,\hat{X}^f_k\right) &\equiv \hat{e}^f - T\hat{s}^f = -\frac{p}{\rho^f} + \sum \hat{\mu}^f_i \hat{X}^f_i,\\
\hat{g}^f(p,T,\hat{X}^f_1,\ldots,\hat{X}^f_k) &\equiv \hat{e}^f - T\hat{s}^f + \frac{p}{\rho^f} = \sum \hat{\mu}^f_i \hat{X}^f_i,
\end{aligned} \tag{2.5}$$

where p is bulk fluid pressure; $\hat{X}^\alpha_i$ is the mass fractions of species i in phase α; $\hat{s}^\alpha$ is the mass-specific entropy; T is the absolute temperature. The right-hand side of equation (2.3) or (2.4) indicates that the internal energy of the REV can be altered via mechanical work done in deforming the solid skeleton (first term) and driving fluid flow through the pore network (second term), energy flux owing to fluid and species movements relative to the solid skeleton (third term) and heat conduction (last term).

The second law should be enforced directly on the mixture as a whole, rather than for individual phases [44]. The local entropy imbalance of the system states [42]

$$\frac{\mathrm{d}^s s}{Et} + s\nabla_x \cdot \mathbf{v}^s \geq -\nabla_x \cdot \left(\hat{s}^f \hat{\mathbf{w}} + \frac{\mathbf{q}}{T}\right) \text{ or } \frac{\partial S}{\partial t} \geq -\nabla_X \cdot \left(\hat{s}^f \hat{\mathbf{W}} + \frac{\mathbf{Q}}{T}\right), \tag{2.6}$$

where $s = \rho^s(1-n)\hat{s}^s + \rho^f n\hat{s}^f + \rho^e n\hat{s}^e$ and $S = Js$ are the overall entropy per unit current and reference total volume, respectively. Expressing equation (2.4) in terms of Helmholtz free energy using $E = \Psi + ST$ and combining with equation (2.6), the Lagrangian free energy imbalance (also called the Clausius–Duhem inequality) of the mixture is derived as

$$\Phi = \mathbf{S} : \frac{\partial \mathbf{E}}{\partial t} + (\mathbf{f} - \mathbf{a}^f) \cdot \mathbf{F} \cdot \hat{\mathbf{W}} - \sum \nabla_X \cdot \hat{\mu}^f_i \hat{\mathbf{W}}_i + \left(-\frac{\mathbf{Q}}{T} - \hat{s}^f \hat{\mathbf{W}}\right) \cdot \nabla_X T - S\frac{\partial T}{\partial t} - \frac{\partial \Psi}{\partial t} \geq 0, \tag{2.7}$$

where Φ is the overall energy dissipation in the REV; $\hat{\mathbf{w}}_i = M_i n^f_i (\mathbf{v}^f_i - \mathbf{v}^s)$ and $\hat{\mathbf{W}}_i = J\mathbf{F}^{-1} \cdot \hat{\mathbf{w}}_i$ are the Eulerian and Lagrangian relative species–solid flow vectors by mass, respectively. The relation between the different relative flow vectors $\hat{\mathbf{W}}_i$, $\hat{\mathbf{H}}_i$ and $\hat{\mathbf{W}}_i$ are given in electronic supplementary material, eqn. (A.7). Equation (2.7) sets the directionality for all processes occurring within the multicomponent-fluid saturated porous medium, whether inert or chemically active. Any proposed constitutive models, reaction kinetics or transport models for this material system must not violate this general thermodynamic constraint.

3. Transport, kinetic and constitutive laws

Substituting the averaging relation and the mole balances (electronic supplementary material, eqns. (A.6), (A.5) and (A.4)), the free energy imbalance equation (2.7) can be rewritten as

$$\Phi = \Phi_M + \Phi_R + \Phi_H + \Phi_C + \Phi_T \geq 0, \tag{3.1}$$

where

$$\Phi_M = \mathbf{S} : \frac{\partial \mathbf{E}}{\partial t} + \hat{g}^f \frac{\partial \rho^f \phi}{\partial t} + \sum \rho^f \phi \hat{\mu}^f_i \frac{\partial \hat{X}^f_i}{\partial t} + \sum M_i \hat{\mu}^e_i \frac{\partial N^e_i}{\partial t} - S\frac{\partial T}{\partial t} - \frac{\partial \Psi}{\partial t} \tag{3.2}$$

is the material dissipation rate;

$$\Phi_R = -\sum_{\alpha=f,e} \sum_{i=1}^{k} \hat{\mu}^\alpha_i \hat{R}^\alpha_i \tag{3.3}$$

Downloaded from http://royalsocietypublishing.org/rspa/article-pdf/doi/10.1098/rspa.2025.1094/6136174/rspa.2025.1094.pdf
by guest
on 07 May 2026

is the reaction dissipation rate; and

$$\Phi_H = \left[-\nabla_X \hat{g}^f - \hat{s}^f \nabla_X T + (\mathbf{f} - \mathbf{a}^f) \cdot \mathbf{F} + \sum \hat{\mu}_i^f \nabla_X \hat{X}_i^f\right] \cdot \hat{\mathbf{W}},$$
$$\Phi_C = -\sum \hat{\mathbf{H}}_i \cdot \nabla_X \hat{\mu}_i^f,$$
$$\Phi_T = -\frac{\mathbf{Q}}{T} \cdot \nabla_X T, \tag{3.4}$$

are the dissipation rates related to thermal conduction, species diffusion and fluid transport. The material, reaction and transport dissipations identified in equation (3.1) correspond to relatively independent, individually controllable processes. Therefore, equation (3.1) can be replaced by a stricter condition:

$$\Phi_M \geq 0,\ \Phi_R \geq 0,\ \Phi_H + \Phi_C + \Phi_T \geq 0. \tag{3.5}$$

(a) Transport laws and reaction kinetics

The consequences of transport dissipation $\Phi_H + \Phi_C + \Phi_T \geq 0$ have been discussed in Zhang [26] and are not revisited here. In brief, this inequality is satisfied by a linear conduction law with a positive semi-definite transport matrix, i.e. a generalized Darcy–Fourier–Fick law.

The reaction dissipation is new in the current derivation, as we considered a chemically active system. In this study, 'reaction' refers specifically to sorption, that is, the uptake of species by the solid skeleton through either physical interactions (e.g. van der Waals or electrostatic forces) or chemical reactions (involving electron sharing/transfer and bond formation). The stoichiometry of sorption can be expressed as

$$\frac{R_i^f}{\Upsilon_i^f} = \frac{R_i^e}{\Upsilon_i^e} = R_i \text{ for } i = 1, 2, \ldots, k, \tag{3.6}$$

where Υ_i^α is the stoichiometry coefficient which equals -1 for the bulk fluid and $+1$ for the excess phase; R_i is the reaction (sorption) rate. Substituting equation (3.6) into equation (3.3) gives

$$\Phi_R = -\sum_{\alpha=f,e} \sum_{i=1}^{k} \hat{\mu}_i^\alpha M_i \Upsilon_i^\alpha R_i = \sum_{i=1}^{k} \overbrace{(\mu_i^f - \mu_i^e)}^{\mathrm{A}_i} R_i \geq 0, \tag{3.7}$$

where $\mu_i^\alpha = M_i \hat{\mu}_i^\alpha$ is the molar chemical potential; $\mathrm{A}_i = \mu_i^f - \mu_i^e$ is the chemical affinity, which serves as the thermodynamic driving force of chemical reaction R_i. For the system considered here, $\mathrm{A}_i > 0$ indicates the tendency of sorption, $\mathrm{A}_i < 0$ for desorption and chemical equilibrium is attained at $\mathrm{A}_i = 0$. The simplest sorption kinetics that satisfies constraint equation (3.7) is a linear one, with the pre-factor scales with temperature through an Arrhenius term:

$$\mathrm{A}_i = \xi R_i \exp\left(\frac{E_a}{R_g T}\right), \tag{3.8}$$

where $\xi \geq 0$ is a sorption rate constant; E_a is the activation energy; R_g is the gas constant.

We can see that the overall transient behaviours of the system are governed by two rate-limiting processes: mass transport in across domain Ω_t described by the generalized Darcy–Fourier–Fick law and the rate of phase transition of species i from the free bulk fluid phase to the immobile excess phase described by the sorption kinetics equation (3.8). For nanoporous media, the equilibrium time is primarily governed by the rate of mass transport, and the local sorption/desorption kinetics can be assumed instantaneous [45]. Therefore, we assume that local chemical equilibrium $\mathrm{A}_i = 0$ or $\mu_i^f = \mu_i^e = \mu_i$ is always guaranteed. Hereafter, we use μ_i and $\hat{\mu}_i$ without the superscripts e and f to represent the molar- and mass- specific chemical potentials.

Downloaded from http://royalsocietypublishing.org/rspa/article-pdf/doi/10.1098/rspa.2025.1094/6136174/rspa.2025.1094.pdf
by guest
on 07 May 2026

(b) Constitutive relations

Material dissipation Φ_M characterizes energy loss associated with the change of states of the constituents of the REV, including the solid, the fluid and the excess phases. It encompasses all inelastic processes such as viscoelasticity, viscoplasticity, damage, fracture and hysteresis happening at micro-, meso- and macroscales in the REV. To further decompose equation (3.2) into a form that facilitates the discussion of the constitutive and state equations of each phase, it is helpful to define the mass-specific enthalpy $\hat{h}^e$, Helmholtz free energy $\hat{\psi}^e$ and Gibbs free energy $\hat{g}^e$ of the excess phase, in direct analogy with the bulk-fluid energy potentials in equation (2.5), as

$$\begin{cases} \hat{h}^e(\Pi, \hat{s}^e, \hat{X}^e_1, \ldots, \hat{X}^e_k) \equiv \hat{e}^e + \frac{\Pi}{\rho^e} = T\hat{s}^e + \sum \hat{\mu}^e_i \hat{X}^e_i, \\ \hat{\psi}^e\left(\frac{1}{\rho^e}, T, \hat{X}^e_1, \ldots, \hat{X}^e_k\right) \equiv \hat{e}^e - T\hat{s}^e = -\frac{\Pi}{\rho^e} + \sum \hat{\mu}^e_i \hat{X}^e_i, \\ \hat{g}^e(\Pi, T, \hat{X}^e_1, \ldots, \hat{X}^e_k) \equiv \hat{e}^e + \frac{\Pi}{\rho^e} - T\hat{s}^e = \sum \hat{\mu}^e_i \hat{X}^e_i, \end{cases} \tag{3.9}$$

where Π is a new pressure-like term conjugate to the density change of the excess phase, which will be elaborated further later. Thermodynamically conjugate (also called dual or work-conjugate) variables are pairs whose inner product gives the rate of work or dissipation [9].

Combining equations (2.5) and (3.9), the material dissipation equation (3.2) can be rewritten as

$$\Phi_M = \Phi^s_M + \Phi^f_M + \Phi^e_M \geq 0, \tag{3.10}$$

where

$$\Phi^s_M = \mathbf{S} : \frac{\partial \mathbf{E}}{\partial t} + (p + \Pi)\frac{\partial \phi}{\partial t} - S^s \frac{\partial T}{\partial t} - \frac{\partial \Psi^s}{\partial t}, \tag{3.11}$$

$$\Phi^f_M = \rho^f \phi \left[-p \frac{\partial}{\partial t}\left(\frac{1}{\rho^f}\right) + \sum \hat{\mu}_i \frac{\partial \hat{X}^f_i}{\partial t} - \hat{s}^f \frac{\partial T}{\partial t} - \frac{\partial \hat{\psi}^f}{\partial t} \right] \tag{3.12}$$

and

$$\Phi^e_M = \rho^e \phi \left[-\Pi \frac{\partial}{\partial t}\left(\frac{1}{\rho^e}\right) + \sum \hat{\mu}_i \frac{\partial \hat{X}^e_i}{\partial t} - \hat{s}^e \frac{\partial T}{\partial t} - \frac{\partial \hat{\psi}^e}{\partial t} \right], \tag{3.13}$$

are the material dissipations associated with the solid, the bulk fluid and the sorbed excess phases, respectively; Ψ^s is the volume-specific Helmholtz free energy of the porous solid defined by

$$\Psi \equiv \Psi^s + \rho^f \phi \hat{\psi}^f + \rho^e \phi \hat{\psi}^e, \tag{3.14}$$

similar to E and S in equations (2.4) and (2.6).

(i) Constitutive laws for the porous skeleton

For elastic solid (i.e. $\Phi^s_M = 0$), equation (3.11) reduces to the free energy balance of the porous skeleton:

$$\mathrm{d}\Psi^s = \mathbf{S} : \mathrm{d}\mathbf{E} + \overbrace{(p + \Pi)}^{p^p} \mathrm{d}\phi - S^s \mathrm{d}T, \tag{3.15}$$

where $p^p \equiv p + \Pi$ represents the equivalent pore pressure, i.e. the pore pressure experienced by the skeleton owing to both bulk fluid infiltration and the sorbed excess resulting from the affinity between fluid and solid molecules. The constitutive relations for a sorptive poroelastic material can be deduced from equation (3.15) as

$$\mathbf{S} = \frac{\partial \Psi^s}{\partial \mathbf{E}}; \quad p^p = \frac{\partial \Psi^s}{\partial \phi}. \tag{3.16}$$

Comparing equation (3.15) to its counterpart for fluid-saturated, inert porous media (e.g. eqn. (4.1) in Coussy [42]), it becomes evident that the thermodynamic driving force for porosity evolution now comprises not only the conventional bulk pressure p but also the new term Π introduced by the sorbed excess. Indeed, Π is the so-called *disjoining pressure* [46] or *solvation*

Downloaded from http://royalsocietypublishing.org/rspa/article-pdf/doi/10.1098/rspa.2025.1094/6136174/rspa.2025.1094.pdf
by guest
on 07 May 2026

pressure [1,47] in surface science and material science literature. Its physicochemical origin lies in molecular-scale interactions within the confined fluid, including van der Waals and electric double-layer forces (collectively described by Derjaguin–Landau–Verwey–Overbeek (DVLO) theory), hydration forces arising from water binding to solid surfaces and structural forces resulting from the ordering of fluid molecules near interfaces [48,49]. In studying the energetics of thin liquid films [36] and slit pores [50], disjoining pressure was introduced through an extra work term in bringing two interfaces together down to nanometre separations. In the current derivation (i.e. equation (3.9)), we proved that the disjoining pressure for a macroscopic porous REV is a property of the excess mass entering the pore space, leading to an overall higher repulsive force exerted on the pore wall compared to that without sorption.

(ii) State equations of the bulk fluid and the excess phases

Considering $\Phi_M^f = \Phi_M^e = 0$, equations (3.13) and (3.12) give the free energy balance of the bulk fluid and excess phases

$$\begin{aligned} \mathrm{d}\hat{\psi}^f &= -p d(1/\rho^f) + \sum \hat{\mu}_i \mathrm{d}\hat{X}_i^f - \hat{s}^f \mathrm{d}T, \\ \mathrm{d}\hat{\psi}^e &= -\Pi d(1/\rho^e) + \sum \hat{\mu}_i \mathrm{d}\hat{X}_i^e - \hat{s}^e \mathrm{d}T, \end{aligned} \tag{3.17}$$

which is consistent with equations (2.5) and (3.9). The equation of state (EOS) of two phases can be deduced as

$$p = -\frac{\partial \hat{\psi}^f(\rho^f, \hat{X}_1^f, \ldots \hat{X}_k^f, T)}{\partial(1/\rho^f)}; \; \Pi = -\frac{\partial \hat{\psi}^e(\rho^e, \hat{X}_1^e, \ldots \hat{X}_k^e, T)}{\partial(1/\rho^e)}. \tag{3.18}$$

For a unary fluid, the second equation relates disjoining pressure and excess density $\Pi(\rho^e, T)$, which is referred to as the *disjoining pressure isotherm* hereafter.

(iii) Sorption isotherm

Equations (3.13) and (3.12) can also be rewritten in terms of volume-specific quantities by substituting $s^\alpha = \rho^\alpha \hat{s}^\alpha$, $\psi^\alpha = \rho^\alpha \hat{\psi}^\alpha$, $\mu_i = M_i \hat{\mu}_i$, equation (A.6) in the electronic supplementary material, equations (2.5) and (3.9) for $\alpha = f, e$:

$$\Phi_M^\alpha = \phi \left[\sum \mu_i \frac{\partial}{\partial t} \left(\frac{N_i^\alpha}{\phi} \right) - s^\alpha \frac{\partial T}{\partial t} - \frac{\partial \psi^\alpha}{\partial t} \right]. \tag{3.19}$$

For $\Phi_M^\alpha = 0$, equation (3.19) gives

$$\mathrm{d}\psi^\alpha = \sum \mu_i \mathrm{d}C_i^\alpha - s^\alpha \mathrm{d}T, \tag{3.20}$$

where

$$C_i^\alpha = \frac{N_i^\alpha}{\phi} = \frac{n_i^\alpha}{n} \tag{3.21}$$

is the number of species i in $\alpha = f, e$ phase per unit current pore volume, or simply *concentration*.

An important implication of equation (3.20) is a relation between the excess concentration C_i^e and μ_i:

$$\mu_i = \frac{\partial \psi^e}{\partial C_i^e} = \frac{\partial \psi^f}{\partial C_i^f}. \tag{3.22}$$

This is essentially the sorption isotherm $C_i^e(\mu_i, T)$ that characterizes the affinity of the sorbate to the sorbent at a given temperature T. For a unary fluid, μ is uniquely related to the bulk fluid pressure p. Therefore, the sorption isotherm often takes the form of $C^e(p, T)$.

Equations (3.18) and (3.22) confirm a profound connection between the disjoining pressure isotherm $\Pi(\rho^e, T)$ and the sorption isotherm $C^e(p, T)$ for a unary fluid: they are fundamentally the two sides of the same coin, both are fully defined by the Helmholtz free energy of the excess phase [51]. Disjoining pressure is the thermodynamic conjugate of the excess density, while chemical potential is conjugate to the excess concentration. In §4, we show how equations (3.18) and (3.22)

Downloaded from http://royalsocietypublishing.org/rspa/article-pdf/doi/10.1098/rspa.2025.1094/6136174/rspa.2025.1094.pdf
by guest
on 07 May 2026

can be used to obtain a thermodynamically consistent set of $\Pi(\rho^{\mathrm{e}}, T)$ and $C^{\mathrm{e}}(p, T)$ expressions governed by the same parameters and highlight their remarkable predictive capabilities.

(c) An alternative two-phase formulation

One may opt to combine equations (3.13) and (3.12) to interpret the combined excess and the bulk fluid phase as a whole:

$$\Phi_M^p = \Phi_M^f + \Phi_M^e = \phi\left[\sum \mu_i \frac{\partial}{\partial t}\left(\frac{N_i^p}{\phi}\right) - s^p\frac{\partial T}{\partial t} - \frac{\partial \psi^p}{\partial t}\right], \tag{3.23}$$

where $(\cdot)^p = (\cdot)^{\mathrm{f}} + (\cdot)^{\mathrm{e}}$ and superscript p stands for a lumped 'pore fluid' phase. Setting $\Phi_M^p = 0$ gives

$$\mathrm{d}\psi^p = \sum \mu_i \mathrm{d}C_i^p - s^p \mathrm{d}T, \tag{3.24}$$

which is similar to that of the separated phases equation (3.20). It leads to a combined sorption isotherm in the form of $\mu_i = \partial\psi^p/\partial C_i^p$.

Similarly, we can define the density, mass-specific entropy and mass-specific free energy of the p phase as

$$\rho^p \equiv \frac{1}{\phi}\sum M_i N_i^p = \frac{1}{\phi}\sum M_i N_i^f + \frac{1}{\phi}\sum M_i N_i^e = \rho^f + \rho^e, \tag{3.25}$$

$$\hat{s}^p \equiv \frac{s^p}{\rho^p} = \frac{\rho^f \hat{s}^f + \rho^e \hat{s}^e}{\rho^f + \rho^e}; \quad \hat{\psi}^p \equiv \frac{\psi^p}{\rho^p} = \frac{\rho^f \hat{\psi}^f + \rho^e \hat{\psi}^e}{\rho^f + \rho^e}. \tag{3.26}$$

Substituting equations (2.5) and (3.9) into equation (3.26) gives

$$\hat{\psi}^p = -\frac{1}{\rho^p}\overbrace{(p + \Pi)}^{p^p} + \sum \hat{\mu}_i \hat{X}_i^p - \hat{s}^p \mathrm{d}T, \tag{3.27}$$

where $\hat{X}_i^p = M_i N_i^p/(\rho^p\phi)$. This proves that the equivalent pore pressure p^p introduced in equation (3.15) is indeed the conjugate of pore fluid density:

$$p^p = -\frac{\partial \hat{\psi}^p}{\partial(1/\rho^p)} = -\frac{\partial \hat{\psi}^f}{\partial(1/\rho^f)} - \frac{\partial \hat{\psi}^e}{\partial(1/\rho^e)}. \tag{3.28}$$

It is conceivable that a model developed by treating the bulk fluid and the excess phases separately, based on equations (3.15)–(3.22), can be equivalently rewritten in terms of a single pore fluid phase using equations (3.24)–(3.28). The former may be referred to as the *three-phase formulation* and the latter as the *two-phase formulation*.

(d) Effective stress

For gels and many other polymeric materials, the solid phase is often regarded as incompressible. Under this assumption, we have

$$\mathrm{d}\Omega_t^s = (1-n)\mathrm{d}\Omega_t = (J-\phi)\mathrm{d}\Omega_0 = (1-\phi_0)\mathrm{d}\Omega_0, \tag{3.29}$$

where ϕ_0 is the initial porosity. This implies

$$n = 1 - \frac{1-\phi_0}{J}; \quad \phi = \phi_0 + J - 1; \quad dJ = d\phi. \tag{3.30}$$

Substituting equation (3.30) into equation (3.11) and considering relations $\mathbf{S}:\dot{\mathbf{E}} = J\boldsymbol{\sigma}:\mathbf{D}$ and $Jtr\mathbf{D} = \dot{J}$ [52], Φ_M^s can be rewritten as

$$\Phi_M^s = J\overbrace{[\boldsymbol{\sigma} + (p+\Pi)\mathbf{I}]}^{\boldsymbol{\sigma}'}:\mathbf{D} - S^s\frac{\partial T}{\partial t} - \frac{\partial \Psi^s}{\partial t}, \tag{3.31}$$

Downloaded from http://royalsocietypublishing.org/rspa/article-pdf/doi/10.1098/rspa.2025.1094/6136174/rspa.2025.1094.pdf
by guest
on 07 May 2026

where

$$\boldsymbol{\sigma}' = \boldsymbol{\sigma} + p^p \mathbf{I} = \boldsymbol{\sigma} + (p + \Pi)\mathbf{I} \tag{3.32}$$

is the effective stress. Equation (3.32) degenerates to Terzaghi's effective stress in the absence of sorption (i.e. $\Pi = 0$). Again, we observe that in sorptive porous media, the pore pressure must be the sum of the bulk fluid pressure and the disjoining pressure contributed by the additional fluid mass retained in the pore space. Note that the effective stress equation (3.32) emerges directly from the proposed theory under the incompressibility condition, rather than being assumed *a priori* as in Bertrand *et al.* [53].

4. A simple constitutive model for swelling nanoporous solids

(a) Effective stress formulation

To demonstrate the workflow of constructing a constitutive model within the proposed poromechanics framework, this section introduces a simple, effective-stress-based model for the mechano-sorptive behaviour of AC immersed in water vapour. In this system, the solid (s) phase consists of cellulose chains, the bulk fluid (f) phase is water vapour and the excess (e) phase represents additional water captured in the pore space beyond the vapour state. The number of fluid species is $k = 1$, since only water molecules are present. The analysis will focus on isothermal conditions ($dT = 0$), for which T is excluded from the list of variables in the energy potentials.

(i) Solid skeleton

Equation (3.31) defines the constitutive law of the elastic porous solid ($\Phi_M^s = 0$) in terms of effective stress:

$$\mathbf{S}' = \frac{\partial \Psi^s(\mathbf{E})}{\partial \mathbf{E}} = 2\frac{\partial \Psi^s(\mathbf{C})}{\partial \mathbf{C}}, \tag{4.1}$$

where $\mathbf{S}' = J\mathbf{F}^{-1} \cdot [\boldsymbol{\sigma} + (p + \Pi)\mathbf{I}] \cdot \mathbf{F}^{-T}$ is the effective Second Piola–Kirchhoff stress; $\mathbf{C} = \mathbf{F}^T \cdot \mathbf{F}$ is the right Cauchy–Green tensor. The simplest choice of Ψ^s is the compressible neo-Hookean potential [43]:

$$\Psi^s(\mathbf{C}) = \frac{G}{2}\left[(I_1 - 3) + \frac{2}{\beta}(J^{-\beta} - 1)\right], \tag{4.2}$$

where G and β control the apparent shear and bulk modulus, respectively; $I_1 = tr\mathbf{C}$ is the first invariant of $\mathbf{C}$. Substituting equation (4.2) into equation (4.1) gives

$$\mathbf{S}' = G(\mathbf{I} - J^{-\beta}\mathbf{C}^{-1}) \quad \text{or} \quad \boldsymbol{\sigma}' = J^{-1}G(\mathbf{B} - J^{-\beta}\mathbf{I}), \tag{4.3}$$

where $\mathbf{B} = \mathbf{F} \cdot \mathbf{F}^T$ is the left Cauchy–Green tensor. As discussed in §3d, the adoption of effective stress implies an incompressible solid phase. Consequently, the evolution of porosity is entirely governed by equation (3.30).

(ii) Bulk fluid

We approximate water vapour (i.e. the f phase) as an ideal gas here for its simplicity. Its Helmholtz free energy in volume- and mass-specific forms can be expressed as

$$\psi^f = R_g T C^f \ln\left(\frac{C^f}{C_r^f}\right); \quad \hat{\psi}^f(\rho^f) = \frac{R_g T}{M} \ln\left(\frac{\rho^f}{\rho_r^f}\right), \tag{4.4}$$

where $R_g = 8.314\,\mathrm{J/K\,mol}$ is the gas constant; $T = 300\,\mathrm{K}$ is the temperature; $M = 18\,\mathrm{g\,mol^{-1}}$ is the molar mass of water; ρ_r^f and C_r^f are the density and concentration of the fluid at an arbitrary

Downloaded from http://royalsocietypublishing.org/rspa/article-pdf/doi/10.1098/rspa.2025.1094/6136174/rspa.2025.1094.pdf
by guest
on 07 May 2026

reference state, respectively. Consulting equations (3.22) and (3.18), we have

$$\mu = \frac{\partial \psi^f}{\partial C^f} = R_g T + R_g T \ln\left(\frac{C^f}{C_r^f}\right) \tag{4.5}$$

and

$$p = -\frac{\partial \hat{\psi}^f(\rho^f)}{\partial 1/\rho^f} = \frac{R_g T}{M}\rho^f = R_g T C^f. \tag{4.6}$$

Equation (4.6) is the familiar ideal gas law depicting a linear pressure–concentration relation. Substituting equation (4.6) into equation (4.5) yields the relationship between pressure and chemical potential for water vapour:

$$\mu = \mu_0 + R_g T \ln\left(\frac{p}{p_{\text{sat}}}\right), \tag{4.7}$$

where $p_{\text{sat}} = 3527$ Pa is the saturated vapour pressure at a given condition; $\mu_0 = R_g T[1 + \ln(p_{\text{sat}}/p_r)]$ is a reference chemical potential; $p_r = R_g T C_r^f$ is the pressure at the reference state.

(iii) Sorbed excess

For the excess (e) phase, let us propose the following volume-specific Helmholtz free energy:

$$\psi^e(C^e) = R_g T C^e + R_g T C^e \ln\left[\frac{C^e}{Bp_r(C_0 - C^e)}\right] + R_g T C_0 \ln\left(\frac{C_0 - C^e}{C_0}\right), \tag{4.8}$$

where B and C_0 are model parameters. The sorption isotherm can be readily derived from equation (3.22) as

$$\mu = \frac{\partial \psi^e}{\partial C_i^e} = R_g T + R_g T \ln\left(\frac{C^e}{Bp_r(C_0 - C^e)}\right). \tag{4.9}$$

Substituting equation (4.7) into equation (4.9) and rearranging gives

$$C^e = \frac{C_0 B p}{1 + Bp}. \tag{4.10}$$

This is the well-known Langmuir isotherm used to describe monolayer sorption or nanoscale sorption phenomena [54], which is appropriate for the nanoporous material discussed here. More elaborate sorption models (e.g. BET, BDDT, GAB) [55–57] can be incorporated straightforwardly, if needed, by adopting alternative expressions for ψ^e.

Converting equation (4.8) to mass-specific form yields

$$\hat{\psi}^e = \frac{\psi^e}{\rho^e} = \frac{R_g T}{M} + \frac{R_g T}{M} \ln\left[\frac{\rho^e}{Bp_r(MC_0 - \rho^e)}\right] + \frac{R_g T C_0}{\rho^e} \ln\left(1 - \frac{\rho^e}{MC_0}\right). \tag{4.11}$$

The disjoining pressure can be derived using equation (3.18) as

$$\Pi = -\frac{\partial \hat{\psi}^e}{\partial(1/\rho^e)} = R_g T C_0 \ln\left(\frac{MC_0}{MC_0 - \rho^e}\right) = R_g T C_0 \ln\left(\frac{C_0}{C_0 - C^e}\right). \tag{4.12}$$

Combining equations (4.10) and (4.12) gives the disjoining pressure isotherm in terms of vapour pressure:

$$\Pi = R_g T C_0 \ln(1 + Bp). \tag{4.13}$$

Note that parameters B and C_0 govern both the sorption isotherm equation (4.10) and the disjoining pressure isotherm equation (4.13), as they are both fundamentally derived from the Helmholtz free energy of the excess phase. Figure 3 plots them as functions of relative humidity (RH) $RH = p/p_{\text{sat}}$ at different B and C_0 values.

Downloaded from http://royalsocietypublishing.org/rspa/article-pdf/doi/10.1098/rspa.2025.1094/6136174/rspa.2025.1094.pdf
by guest
on 07 May 2026

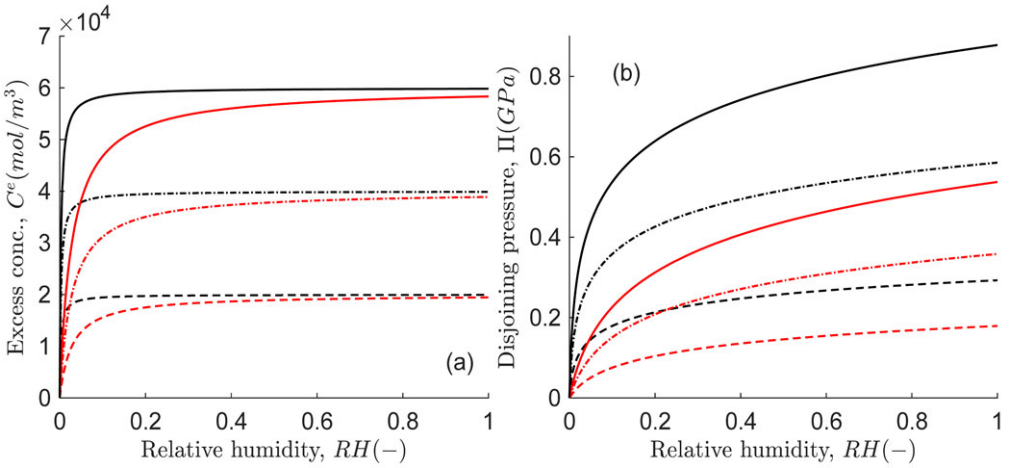

Figure 3. (a) Sorption and (b) disjoining pressure isotherms at different values of B (red = 0.01, black = 0.1, unit Pa^{-1}) and C_0 (dashed line = 2e4, dashed dot = 4e4, solid line=6e4, unit mol m^{-13}).

(iv) Summary

Combining equations (3.32), (4.3), (4.6), (4.10) and (4.13), the derived effective-stress-based constitutive model can be summarized as

$$\begin{cases} \boldsymbol{\sigma} = J^{-1}G(\mathbf{B} - J^{-\beta}\mathbf{I}) - [p + R_g T C_0 \ln(1 + Bp)]\mathbf{I}, \\ \phi = \phi_0 + J - 1, \\ N^p = \phi(C^f + C^e) = \left(1 + \dfrac{R_g T C_0 B}{1 + Bp}\right)\dfrac{\phi p}{R_g T}. \end{cases} \tag{4.14}$$

The model contains only four parameters, each with a clear physical interpretation and calibratable through routine laboratory tests (see the next section). It is remarkable that, although the constitutive ingredients (equations (4.3), (4.6), (4.10)) are intentionally chosen to be decoupled, textbook-level models, the resulting model (equation (4.14)) exhibits a complex two-way coupling: the stress–strain relation depends on sorption properties, while the sorption isotherm is influenced by porosity. No extra parameters are introduced to fine tune this coupling. Instead, it naturally emerges from the thermodynamic relationships among effective stress, disjoining pressure and sorption isotherms. One may turn off sorption by setting $C_0 = 0$, and equation (4.14) immediately reduces to a finite-strain poroelasticity model for non-sorptive porous materials.

In principle, the proposed model can be obtained using a two-phase formulation presented in §3c by reverse engineering from the expressions of p^p and C^p given by equation (4.14). However, the expressions of $\psi^p(C^p)$ or $\hat{\psi}^p(\rho^p)$ become highly cumbersome, if not analytically unfeasible, and the physical meaning of each term becomes unintuitive. This highlights the irreplaceable role of the three-phase formulation in preserving the simplicity and modularity of the proposed framework, allowing for the development of specialized constitutive models tailored to different solid–fluid systems.

(b) Model calibration

Since the constitutive model equation (4.14) is the main outcome of the present theoretical development, its calibration and validation will be conducted at the material point or the REV level. Once validated, the proposed model can be readily integrated into a finite-element framework, together with the generalized transport laws, to simulate initial boundary value

Downloaded from http://royalsocietypublishing.org/rspa/article-pdf/doi/10.1098/rspa.2025.1094/6136174/rspa.2025.1094.pdf
by guest
on 07 May 2026

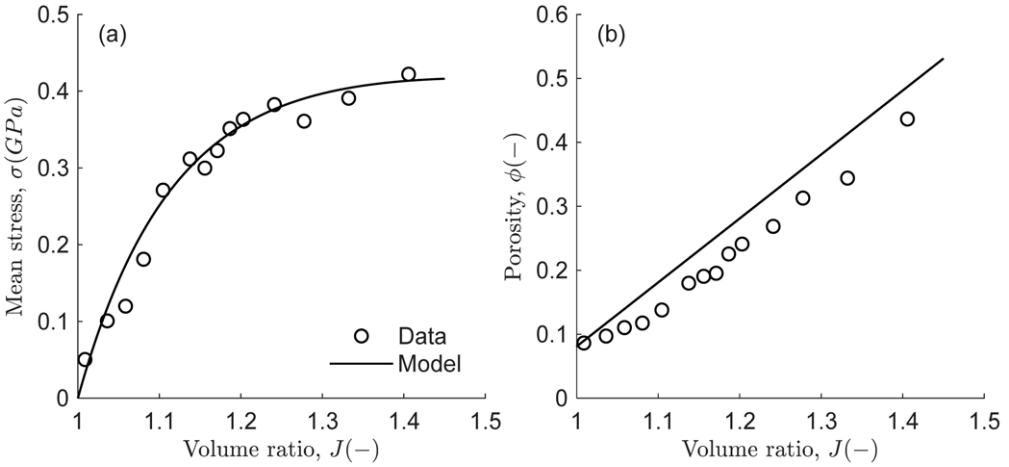

Figure 4. Model versus data during isotropic expansion test at moisture-free condition: (a) $\sigma - J$ curve and (b) $\phi - J$ curve. The volumetric strain data from Chen *et al*. [2] are converted to J via $J = (1 + \varepsilon/3)^3$.

problems involving coupled swelling, species migration and heat conduction processes similar to other works [58–60]. In a series of studies, Chen *et al*. (63,64) extensively investigated the sorption–swelling response of AC using a hybrid molecular dynamic (MD) and grand canonical Monte Carlo (GCMC) approach within the osmotic statistical ensemble ($\mu\sigma T$) at $T = 300\,\mathrm{K}$. Their simulations probed the equilibrium state of a cubical AC specimen at various values of RH (RH) and mechanical conditions including moisture-free isotropic expansion, free swelling, constrained sorption and stressed swelling (figure 1). Therefore, their dataset offers a quantitative benchmark for the two-way coupled sorption–deformation behaviour results purely from the constitutive properties, isolating the transient effects generated from the transport process. This provides a unique opportunity for the calibration and validation of the proposed constitutive model.

First, the mechanical parameters (G, β) can be calibrated using data from isotropic expansion test under moisture-free condition. Figure 4a plots the Jacobian or the volume ratio (current volume over reference volume), J, of the AC sample with respect to the mean stress, $\sigma = \mathrm{tr}(\boldsymbol{\sigma})/3$, in the absence of water vapour (i.e. $p = 0\,\mathrm{Pa}$). Figure 4b shows the corresponding porosity evolution during the test. The mechanical parameters $G = 0.5\,\mathrm{GPa}$ and $\beta = 7$ are determined to best match the data. Note that both parameters are determined by matching the initial slope and the curvature of the $\sigma - J$ curve in figure 4a, while the $\phi - J$ curve in figure 4b is entirely governed by the incompressibility condition equation (3.30), with no tunable parameters. We observe that this assumption slightly overpredicts the change of ϕ and cannot capture the subtle nonlinearity of the $\phi - J$ curve at the beginning of the test. This can be addressed using more general nonlinear poroelasticity models equipped with independent porosity laws, as will be demonstrated in §5a. The overall agreement is satisfactory for the purpose here.

Second, the sorption parameters (B, C_0) are best calibrated using data from the free swelling test, where p increases from 0 Pa to saturated vapour pressure $p_{\mathrm{sat}} = 3527\,\mathrm{Pa}$ (at $T = 300\,\mathrm{K}$) while holding total stress constant $\boldsymbol{\sigma} = \mathbf{0}$. Figure 5a plots the apparent concentration of the pore fluid (bulk + excess), N^p, against the relative humidity $RH = p/p_{\mathrm{sat}}$. Figure 5b,c reports how the volume of the specimen changes during sorption in terms of J with respect to RH and N^p, respectively. The calibrated values are $C_0 = 3.745 \times 10^4\,\mathrm{mol\,m^{-3}}$ and $B = 2.3 \times 10^{-2}\,\mathrm{Pa^{-1}}$. The model performs very well across all planes and is particularly notable for accurately capturing the initial nonlinearity in the $J - N^p$ response shown in figure 5c.

Note that, although both figures 4 and 5 are model calibration and therefore a result of fitting, it is not trivial to capture all five plots with a limited number of parameters. This can

Downloaded from http://royalsocietypublishing.org/rspa/article-pdf/doi/10.1098/rspa.2025.1094/6136174/rspa.2025.1094.pdf
by guest
on 07 May 2026

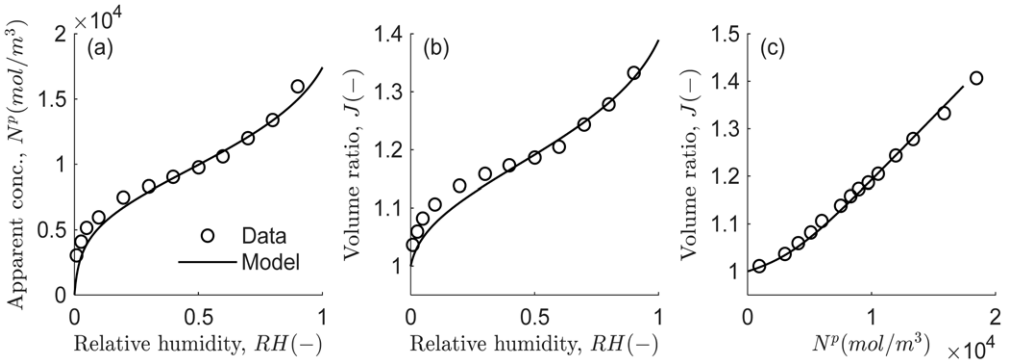

Figure 5. Model versus data during free swelling ($\boldsymbol{\sigma} = \mathbf{0}$) test: (a) $N^p - RH$ response; (b) $J - RH$ response and (c) $J - N^p$ response.

only be achieved by correctly reflecting the underlying physics of sorption–deformation in soft nanoporous materials in the thermodynamic theory. The model of Chen *et al.* [2] performed equally well in capturing these data; however, their model requires five parameters and is limited to isotropic deformation at small strains.

Using the calibrated parameters, we proceed to assess the predictive capability of the model by comparing the predicted sorption–deformation responses under various loading paths with the MD-GCMC simulation results.

(c) Two-way sorption–deformation coupling

One option to probe the coupled behaviour of the REV is through constrained sorption tests (figure 1a), where the relative humidity is increased while maintaining constant volume ($dJ = 0$) on the sample. These tests are conducted at both the initial unswollen state and the fully swollen state. For the latter, the material is first isotropically expanded from $J = 0$ to 1.41 at the moisture-free condition, after which the relative humidity is increased from 0 to 1 with J held constant. Chen *et al.* [2] conducted these tests and interpreted the data using the concept of sorption-induced stress σ_s, which quantifies the deviation of the stress experienced by the solid skeleton from that in the absence of fluid. Comparing this definition to equation (3.32), it is apparent that their σ_s is identical to the equivalent pore pressure p^p in the present effective stress model.

The predicted sorption isotherms and equivalent pore pressure are compared with the MD-GCMC data in figure 6. The agreement between the two is remarkable, especially considering that all parameters were calibrated and fixed previously. The model successfully predicted that, owing to enlarged pore space, the REV at the swollen state can accommodate nearly six times more sorbate molecules compared to the unswollen state. Despite the increased sorption, the model predicts that the swollen state does not generate significantly higher p^p compared to the unswollen state, resulting in a shallower slope on the $p^p - N^p$ plane, which is again corroborated by the data. The ability of the model to capture the nonlinearity of the $p^p - N^p$ response is also noteworthy.

Figures 7a,b show the lumped pore concentration $C^p = N^p/\phi$ and p^p as functions of RH for all three tests: free swelling, constrained sorption in the swollen state and constrained sorption in the unswollen state. On both planes, the MD-GCMC data for all tests approximately collapse into a single characteristic curve. This implies that the pore fluid obeys a single $p - C^p - \Pi$ relation, which is indeed a requirement of the current thermodynamic framework and is accurately captured by the proposed model through equations (4.10) and (4.13). The $C^p - RH$ response is slightly underpredicted owing to the overprediction of porosity change in figure 4b.

Downloaded from http://royalsocietypublishing.org/rspa/article-pdf/doi/10.1098/rspa.2025.1094/6136174/rspa.2025.1094.pdf
by guest
on 07 May 2026

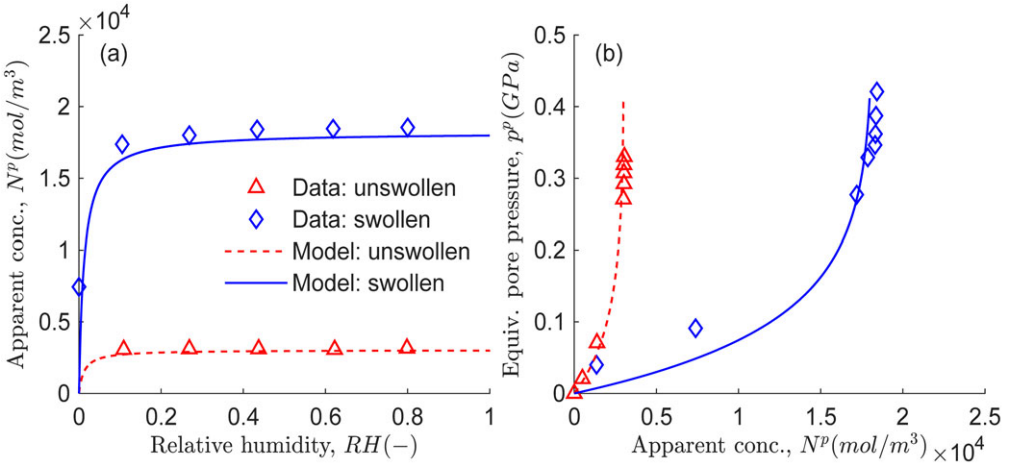

Figure 6. Model versus data for constrained sorption ($dJ = 0$) tests at the initial unswollen state ($J = 0$) and the fully swollen state ($J = 1.41$): (a) $N^p - RH$ response and (b) $p^p - N^p$ response.

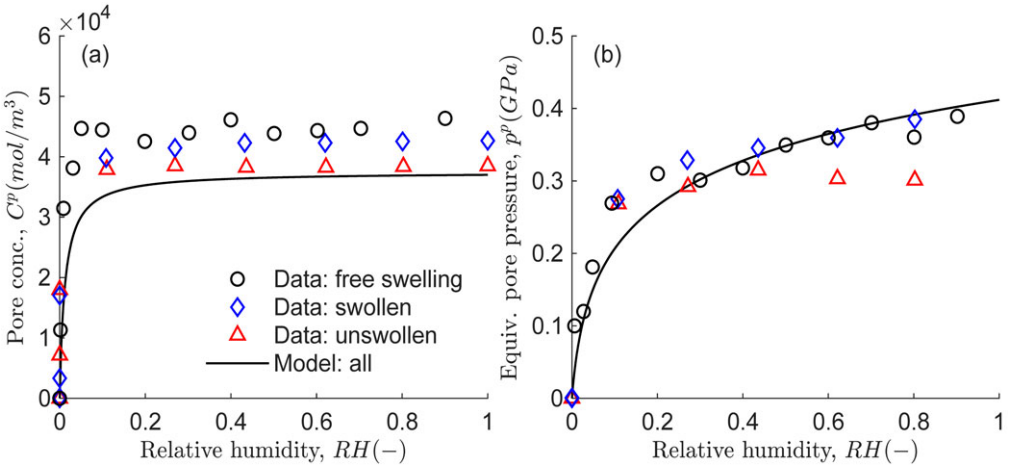

Figure 7. Model versus data for free swelling, constrained sorption in the swollen state and constrained sorption in the unswollen state tests: (a) $C^p - RH$ response and (b) $p^p - RH$ response.

Another way to study sorption–deformation coupling is a stressed swelling test (figure 1a), where the REV is initially isotropically compressed/expanded to a target stress level σ at the moisture-free condition, then σ is held constant while RH is increased from 0 to 1. The model predictions for the stressed swelling test at $\sigma = -10$, 0 and 10 MPa are shown in figure 8 alongside the MD-GCMC results. As seen in figure 8a, the variation of sorption isotherm at different stress levels is well captured by the model. The slight overprediction for the $\sigma = 10$ MPa case could be improved by employing a different hyperelasticity model that offers better control over the $J - \phi - \sigma$ relation. Figure 8b shows that all MD-GCMC data collapse into a nearly linear relation on the $J - N^p$ plane, which is again captured by the current model.

Finally, we highlight that, using the parameters calibrated from the free-swelling tests (figure 5), the sorption–deformation couplings shown in figures 6–8 are all predicted without any additional parameter tuning. The emergence of these couplings from the proposed three-phase poromechanics model, with quantitative agreement against the MD data, is noteworthy.

Downloaded from http://royalsocietypublishing.org/rspa/article-pdf/doi/10.1098/rspa.2025.1094/6136174/rspa.2025.1094.pdf
by guest
on 07 May 2026

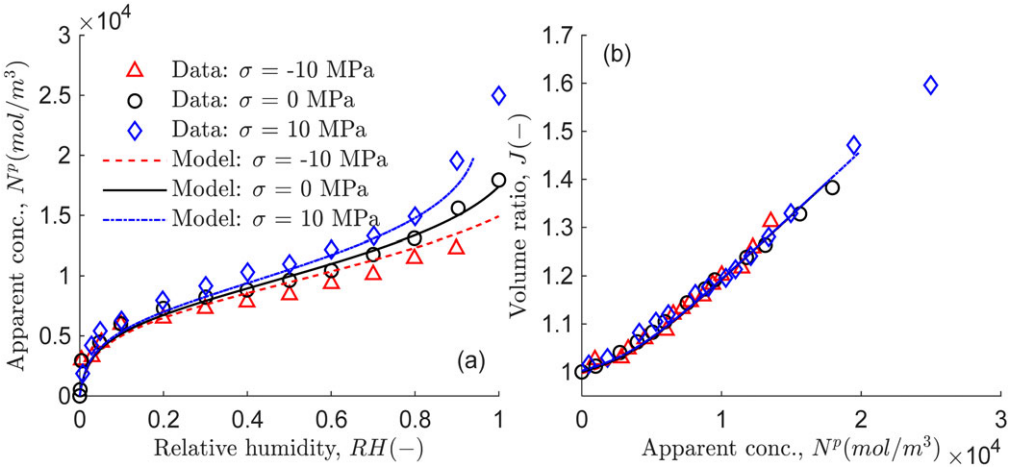

Figure 8. Model versus data for stressed swelling tests at $\sigma = -10$, 0 and 10 MPa: (a) $N^p - RH$ response and (b) $J - N^p$ response.

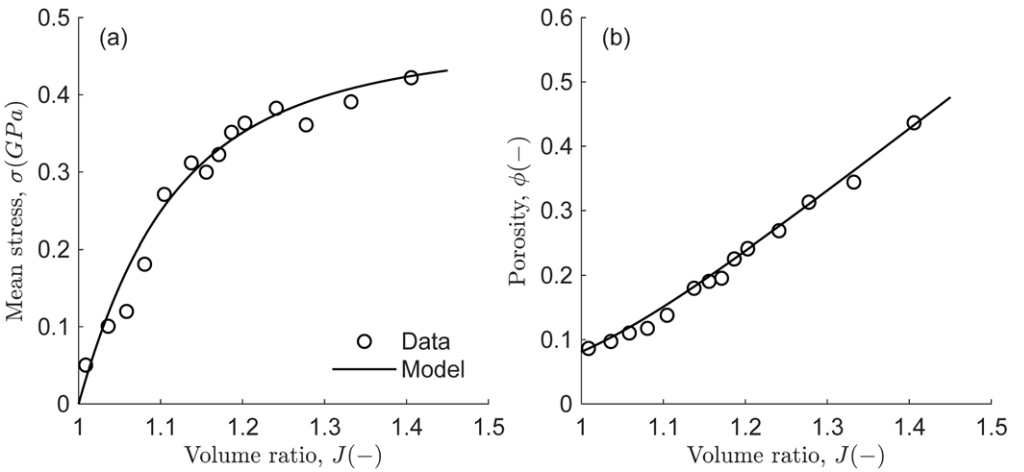

Figure 9. Model versus data during isotropic expansion at $p = 0$: (a) $\sigma - J$ curve and (b) $\phi - J$ curve.

5. Discussions

(a) The general approach

A key advantage of the proposed framework is that it decouples the EOS of the bulk fluid and the sorbed excess from the constitutive response of the porous skeleton. This separation provides great flexibility to tailor individual model components for different material systems. In this section, we leverage this flexibility by relaxing the incompressibility assumption and allowing the solid Helmholtz free energy to depend on both deformation and porosity $\Psi^s(\mathbf{E}, \phi)$. Starting with equation (3.11) and considering again elastic skeleton with unary fluid, the stress–strain and porosity law is given in the coupled form of

$$\mathbf{S} = \frac{\partial \Psi^s(\mathbf{E}, \phi)}{\partial \mathbf{E}} = 2\frac{\partial \Psi^s(\mathbf{C}, \phi)}{\partial \mathbf{C}}; \quad p^p = \frac{\partial \Psi^s(\mathbf{C}, \phi)}{\partial \phi}. \tag{5.1}$$

Downloaded from http://royalsocietypublishing.org/rspa/article-pdf/doi/10.1098/rspa.2025.1094/6136174/rspa.2025.1094.pdf
by guest
on 07 May 2026

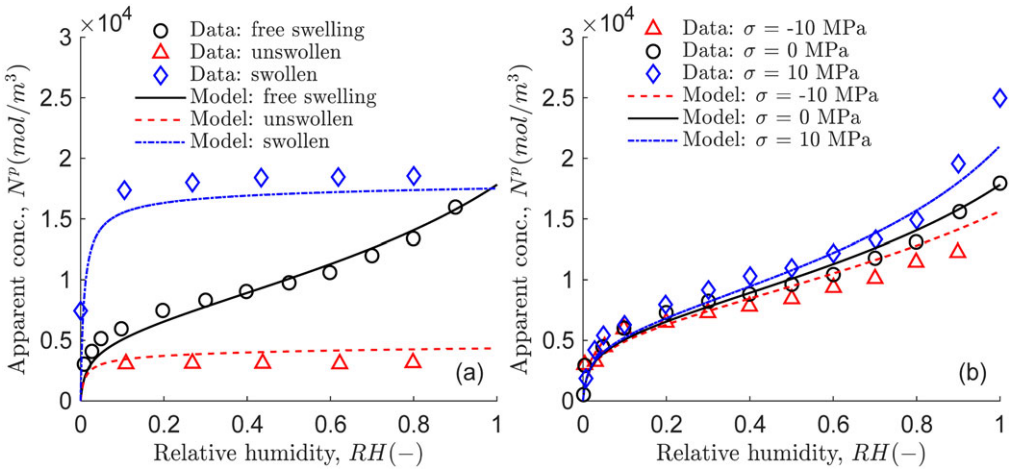

Figure 10. $N^p - RH$ responses predicted by the general model under (a) constrained sorption tests and (b) stressed swelling tests. Results from the free swelling test are included in both figures for reference.

As an example, we consider the following free energy potential modified from Vuong *et al.* [61]:

$$\Psi^s(\mathbf{C},\phi) = \overbrace{\frac{G}{2}\left[(I_1-3)+\frac{2}{\beta}(J^{-\beta}-1)\right]}^{\Psi_{skel}(\mathbf{C})} + \overbrace{\kappa\left[\frac{J-\phi}{1-\phi_0}-1-\ln\left(\frac{J-\phi}{1-\phi_0}\right)\right]+\eta\left[-\ln\left(\frac{\phi}{\phi_0}\right)+\frac{\phi}{\phi_0}-\frac{1}{\phi_0}\right]}^{\Psi_{\text{poro}}(J,\phi)}, \tag{5.2}$$

where $\Psi_{\text{skel}}(\mathbf{C})$ is the skeleton strain energy that takes the same form as equation (4.2); $\Psi_{\text{poro}}(J,\phi)$ corresponds to energy storage owing to porosity change; κ and η are two additional parameters. The constitutive relations are deduced from equations (5.1) and (5.2) as

$$\begin{cases} \mathbf{S} = G(\mathbf{I}-J^{-\beta}\mathbf{C}^{-1}) + \kappa\left(\frac{1}{1-\phi_0}-\frac{1}{J-\phi}\right)J\mathbf{C}^{-1}, \\ p^p = \kappa\left(-\frac{1}{1-\phi_0}+\frac{1}{J-\phi}\right)+\eta\left(-\frac{1}{\phi}+\frac{1}{\phi_0}\right) \end{cases} \tag{5.3}$$

or in Eulerian form

$$\begin{cases} \boldsymbol{\sigma} = J^{-1}\left[G(\mathbf{B}-J^{-\beta}\mathbf{I})+\kappa\left(\frac{J}{1-\phi_0}-\frac{1}{1-n}\right)\mathbf{I}\right], \\ p^p = J^{-1}\left[-\kappa\left(\frac{J}{1-\phi_0}-\frac{1}{1-n}\right)+\eta\left(\frac{J}{\phi_0}-\frac{1}{n}\right)\right]. \end{cases} \tag{5.4}$$

The second relation in equations (5.4) is essentially the porosity law in place of equation (3.30) for the effective-stress-based formulation. We choose to keep the same EOS and sorption isotherm for the f and e phases, as outlined in equations (4.6), (4.10) and (4.13).

Since the total-form constitutive equations (5.4) are expressed in terms of $\mathbf{F}$ and ϕ, it becomes cumbersome if not impossible to simulate sorption tests which are typically p controlled. Results therefore must be obtained using the incremental form of equations (5.4) combined with a numerical integration scheme. Mixed stress–strain–porosity–pressure control can be accomplished through the Bardet–Choucair technique [62]. Details of the incremental formulation as well as the mixed control can be found in electronic supplementary material, §B.

The mechanical parameters are calibrated similarly via dry expansion tests as shown in figure 9. In addition to the expected agreement on the $\sigma - J$ plane, the $\phi - J$ response is now more accurately represented compared to figure 4b. Note that this flexibility to control the $\phi - J$ curve comes at the expense of two extra parameters (κ, η) compared to the effective stress model. The sorption parameters are calibrated using the free swelling data shown in figure 10a. The calibrated parameters are $G = 0.11\,\text{GPa}$, $\beta = 8$, $\kappa = 5.5\,\text{GPa}$, $\eta = 0.033\,\text{GPa}$, $C_0 = 3.525 \times 10^4$

Downloaded from http://royalsocietypublishing.org/rspa/article-pdf/doi/10.1098/rspa.2025.1094/6136174/rspa.2025.1094.pdf
by guest
on 07 May 2026

mol m^{-3} and $B = 6.0 \times 10^{-2}$ Pa^{-1}. The predicted constrained sorption and stressed swelling test results are compiled in figure 10. Figure 10a illustrates that the free swelling response can be interpreted as a scanning curve bridging the two end-member cases: constrained sorption at the unswollen and the fully swollen states, respectively. Overall, similar levels of agreement are observed when comparing figure 10 with figures 6a and 8a, despite the introduction of two additional parameters. This suggests that the four-parameter effective stress approach is more efficient for the AC–water vapour system under study.

(b) Sorption–desorption hysteresis

Note that the MD data used here correspond exclusively to the desorption branch [2]. For cellulose and other nanoporous materials, pronounced sorption–desorption hysteresis is expected and has been reported in other works by Chen *et al*. [63,64].

The current formulation can be readily extended to capture hysteresis. The key is to realize that, when hysteresis is present, each sorption–desorption cycle consumes energy, which can be described by turning on the dissipation term in the free energy imbalances [42]. Specifically, rather than setting $\Phi_M^e = 0$ in equation (3.13) to obtain the reversible sorption–pressure relation, one can enforce a non-negative dissipation and associate it with the rate of change of excess concentration. Rewrite equation (3.13) in volume-specific form equation (3.20) and consider only one species ($k = 1$) for demonstration purpose:

$$\phi\left(\mu\frac{\partial C^e}{\partial t} - s^e\frac{\partial T}{\partial t} - \frac{\partial \psi^e}{\partial t}\right) = \Phi_M^e\left(\frac{\partial C^e}{\partial t}\right) \geq 0. \tag{5.5}$$

Expanding $\psi^{\mathrm{e}}(C^{\mathrm{e}}, T)$ and substituting $s^{\mathrm{e}} = -\partial\psi^{\mathrm{e}}/\partial T$ into equation (5.5) gives

$$\phi\left(\mu - \frac{\partial \psi^e}{\partial C^e}\right)\frac{\partial C^e}{\partial t} = \Phi_M^e\left(\frac{\partial C^e}{\partial t}\right) \geq 0. \tag{5.6}$$

Given ϕ is always positive, this inequality implies that the terms $(\mu - \partial\psi^{\mathrm{e}}/\partial C^{\mathrm{e}})$ and $\partial C^{\mathrm{e}}/\partial t$ must always have the same sign. During desorption where $\partial C^{\mathrm{e}}/\partial t \leq 0$, equation (5.6) suggests that

$$\mu \leq \frac{\partial \psi^e}{\partial C^e}. \tag{5.7}$$

For sorption path where $\partial C^{\mathrm{e}}/\partial t \geq 0$, we have

$$\mu \geq \frac{\partial \psi^e}{\partial C^e}. \tag{5.8}$$

Inequalities (5.7) and (5.8) essentially create distinct sorption and desorption uptake paths at the same RH. Quantitative modelling of hysteresis can be achieved by specifying a proper $\Phi_M^e(\partial C^e/\partial t)$ expression which is not detailed here. The effectiveness of this approach in reproducing typical hysteresis loops has been demonstrated recently for unsaturated mesoporous materials by Behboodi & Zhang [29].

(c) Remarks on the Coussy procedure

The structure of the thermodynamic derivations presented in this paper and in our previous works [26,27] can be collectively referred to as the *Coussy procedure*, as it closely aligns with the spirit of the derivation presented in Coussy [42]. One may have already observed that this procedure is rooted in the mixture theory and the Coleman–Noll method [10,65]. However, Coussy's formulation emphasizes a Lagrangian presentation anchored to the reference configuration of the solid skeleton (e.g. equation (2.4)), with the second law enforced through a single entropy imbalance for the entire system (e.g. equation (2.6)). This differs from mixture theories, which use a more equal and symmetric Eulerian description of all phases. The benefit of the former is that the objectivity principle and the second law can be more straightforwardly fulfilled for developing poromechanics theories. Another major deviation is the treatment of the

Downloaded from http://royalsocietypublishing.org/rspa/article-pdf/doi/10.1098/rspa.2025.1094/6136174/rspa.2025.1094.pdf
by guest
on 07 May 2026

system's free energy imbalance (i.e. equation (2.7)). The Coussy procedure adopts the *postulate of local state* [66] with regard to both time and space, which removes the velocities and spatial gradients from the list of arguments of energy potentials like Ψ and E, significantly simplifying the formulation compared to other mixture theories [44,67]. This also enables the allocation of terms involving velocities and spatial gradients in equation (2.7) to purely dissipative transport-related processes and associates terms containing the rate of change of state variables to the intrinsic material dissipation Φ_M in the system. Furthermore, Coussy decomposed the material dissipation Φ_M to isolate terms related to the state equations of the fluids, so that the free energy imbalance for the remaining porous solid can be discussed in the form of $\Phi_M^s \geq 0$. The elegance of this is that the reversible condition $\Phi_M^s = 0$ naturally yields a linear constitutive model identical to the well-known Biot's theory [68]. Given the infinite ways that Φ_M (equation (3.10)) can be possibly exploited, the chosen decomposition that simultaneously recovers the EOS of the fluids and Biot's theory is certainly elegant and unique.

The Coussy procedure demonstrates remarkable robustness and generality in deriving thermodynamically consistent and practically useful macroscopic theories, spanning from fluid-saturated inert porous solids, as in Coussy *et al.* [17], to chemically active, multicomponent and multiphase porous materials, as presented in this paper and elsewhere [29]. These theories are often connected and consistent with other thermomechanical theories for drastically different systems and processes, as they are rooted in the same fundamental principles. To demonstrate this, the following sections compare the proposed poromechanical framework with several established continuum theories for chemically active materials.

(d) Consistency with the chemomechanics theory of Gurtin *et al.* [9]

It is possible to remove the 'poro' component in the current theory by eliminating the porosity terms in the free energy imbalance. Substituting $\mu_i^\alpha = M_i \hat{\mu}_i^\alpha$, $\hat{X}_i^\alpha = M_i N_i^\alpha / \rho^\alpha \phi$ into equation (3.2) yields

$$\Phi_M = \mathbf{S} : \frac{\partial \mathbf{E}}{\partial t} + \left(\hat{g}^f - \frac{\sum \mu_i^f N_i^f}{\rho^f \phi} \right) \frac{\partial \rho^f \phi}{\partial t} + \sum \mu_i^f \frac{\partial N_i^f}{\partial t} + \sum \mu_i^e \frac{\partial N_i^e}{\partial t} - S \frac{\partial T}{\partial t} - \frac{\partial \Psi}{\partial t}. \tag{5.9}$$

Equation (2.5) suggests that

$$\hat{g}^f = \sum \hat{\mu}_i^f \hat{X}_i^f = \frac{\sum \mu_i^f N_i^f}{\rho^f \phi}. \tag{5.10}$$

Substituting equation (5.10) into equation (5.9) and adopting our previous notations $\mu_i^f = \mu_i^e = \mu_i$ and $N_i^f + N_i^e = N_i^p$ yields

$$\Phi_M = \mathbf{S} : \frac{\partial \mathbf{E}}{\partial t} + \sum \mu_i \frac{\partial N_i^p}{\partial t} - S \frac{\partial T}{\partial t} - \frac{\partial \Psi}{\partial t} \geq 0. \tag{5.11}$$

This is exactly the free energy imbalance of the general chemomechanical theory of Gurtin *et al.* [9] as in equation (1.1), except without the diffusion term which has been separately accounted for in Φ_C in equation (3.4) already. Indeed, equation (5.11) has also been proposed (rather than derived) in Coussy [20] (eqn. (3.69)) and used to guide the development of constitutive models for sorptive materials [13].

Comparing equation (5.11) with equation (3.10), it is evident that poromechanics is a special case of chemomechanics by distinguishing the bulk fluid and the solid phases through introducing volume fractions (i.e. porosity). This point has been well discussed in the Drucker medal paper by Anand [69]. Here, we showed that this conclusion remains valid even for chemically active porous media, where the reaction kinetics equation (3.7) can also be seamlessly deduced from the same free energy imbalance.

Downloaded from http://royalsocietypublishing.org/rspa/article-pdf/doi/10.1098/rspa.2025.1094/6136174/rspa.2025.1094.pdf
by guest
on 07 May 2026

(e) Consistency with the gel mechanics of Hong *et al.* [11]

There are also notable similarities and differences between the gel mechanics of Hong *et al.* [11] and the poromechanics theory proposed here. Specifically, the mechanical consequences of fluid invasion are captured through a free energy of mixing term Ψ_{mix} in gel theory equation (1.2), while the present theory, equation (3.14), distinguishes the solid, fluid and excess phases, along with their respective volume fractions within the mixture. To demonstrate their connections, the first step is to replace porosity by the molar volume ϑ_i^p defined as the apparent pore volume occupied by one mole of species i:

$$\phi = \sum \vartheta_i^p N_i^p. \tag{5.12}$$

Denoting $S^\alpha = \phi s^\alpha$ and $\Psi^\alpha = \phi \psi^\alpha$ as the entropy and free energy of the $\alpha = f, e, p$ phases per unit reference total volume, equation (3.23) can be rewritten as

$$\Phi_M^p = \omega^p \frac{\partial \phi}{\partial t} + \sum \mu_i \frac{\partial N_i^p}{\partial t} - S^p \frac{\partial T}{\partial t} - \frac{\partial \Psi^p}{\partial t}, \tag{5.13}$$

where

$$\omega^p(\mu_i, T) \equiv \psi^p(C_i^p, T) - \sum \mu_i C_i^p \tag{5.14}$$

is the *grand potential* (or the *Landau potential*) of the pore fluid per unit current pore volume. Eliminating ϕ in equation (5.13) by equation (5.12) gives

$$\Phi_M^p = \sum (\omega^p \vartheta_i^p + \mu_i) \frac{\partial N_i^p}{\partial t} + \omega^p \sum N_i^p \frac{\partial \vartheta_i^p}{\partial t} - S^p \frac{\partial T}{\partial t} - \frac{\partial \Psi^p}{\partial t}. \tag{5.15}$$

Summing equations (5.13) and (3.11) provides another form of the material dissipation:

$$\Phi_M = \mathbf{S} : \frac{\partial \mathbf{E}}{\partial t} + (p + \Pi + \omega^p) \frac{\partial \phi}{\partial t} + \sum \mu_i \frac{\partial N_i^p}{\partial t} - S \frac{\partial T}{\partial t} - \frac{\partial \Psi}{\partial t}. \tag{5.16}$$

Comparing equations (5.11) and (5.16) suggests that

$$p + \Pi + \omega^p = 0. \tag{5.17}$$

Combining equations (5.14) and (5.17) reveals the relation

$$g^p \equiv \sum \mu_i C_i^p = p + \Pi + \psi^p, \tag{5.18}$$

where g^p is the Gibbs free energy of the pore fluid per unit current pore volume.

For the special case of unary fluid (i.e. $k = 1$), equations (5.12), (5.14) and (5.18) simplify to

$$\phi = \vartheta^p N^p \quad \text{or} \quad \vartheta^p = \frac{\phi}{N^p} = \frac{1}{C^p}, \tag{5.19}$$

$$\omega^p = \psi^p - \mu C^p = \psi^p - \frac{\mu}{\vartheta^p} \tag{5.20}$$

and

$$g^p = \frac{\mu}{\vartheta^p} = p + \Pi + \psi^p. \tag{5.21}$$

Further assuming reversibility ($\Phi_M^p = 0$), incompressible fluid ($d\vartheta^p = 0$) and isothermal condition ($\mathrm{d}T = 0$), equations (3.11) and (5.15) reduce to

$$\begin{aligned} \mathrm{d}\Psi^s(\mathbf{E}, N^p) &= \mathbf{S} : \mathrm{d}\mathbf{E} + (p + \Pi)\vartheta^p \mathrm{d}N^p, \\ \mathrm{d}\Psi^p(N^p) &= \vartheta^p \psi^p \mathrm{d}N^p. \end{aligned} \tag{5.22}$$

Summing the two and considering equation (5.21) gives the free energy balance of the entire system:

$$\mathrm{d}\Psi(\mathbf{E}, N^p) = \mathbf{S} : \mathrm{d}\mathbf{E} + (p + \Pi + \psi^p)\vartheta^p \mathrm{d}N^p = \mathbf{S} : \mathrm{d}\mathbf{E} + \mu \mathrm{d}N^p. \tag{5.23}$$

One can immediately identify that the first term on the right-hand side of equation (5.23) accounts for the free energy of network stretching and the second term corresponds to the free

Downloaded from http://royalsocietypublishing.org/rspa/article-pdf/doi/10.1098/rspa.2025.1094/6136174/rspa.2025.1094.pdf
by guest
on 07 May 2026

energy of mixing in gel mechanics equation (1.2):

$$\mathrm{d}\Psi_{\mathrm{stretch}}(\mathbf{E}) = \mathbf{S} : \mathrm{d}\mathbf{E};\ \mathrm{d}\Psi_{\mathrm{mix}}(N^p) = \mu \mathrm{d}N^p. \tag{5.24}$$

Therefore, we have proven that the proposed theory is equivalent to the gel theory of Hong *et al.* [11] with the assumption of unary, incompressible fluid. We should caution that $\Psi_{\mathrm{stretch}} \neq \Psi^s$ and $\Psi_{\mathrm{mix}} \neq \Psi^p$ by comparing equation (5.22) and (5.24). This difference stems from the distinct ways in which the chemomechanical and poromechanical formulations decompose Ψ. In the former, the effect of species mixing on the whole REV is of interest, so naturally the second term is entirely attributed to mixing-induced free energy change. In the Coussy procedure, the focus is on separately recovering the EOS of the invading fluids and the constitutive law for the porous skeleton. Therefore, Ψ^s contains elastic energy contributions from both strain and porosity changes.

Combining equation (5.21) and $p^p = p + \Pi$ yields another expression of the equivalent pore pressure in terms of volume-specific quantities:

$$p^p = \frac{\mu}{\vartheta^p} - \psi^p. \tag{5.25}$$

A similar expression was also derived by Bertrand *et al.* [53] for swelling gels via the chemomechanical approach. It is tempting to further claim $p = \mu/\vartheta^p$ or $\Pi = -\psi^p$ by comparing equation (5.25) with $p^p = p + \Pi$. However, this is incorrect since p and Π in the current derivation are explicitly defined as the thermodynamic forces conjugate to the density change of the bulk fluid and the excess phases, respectively. Their expressions can be obtained by converting equations (2.5) and (3.9) to volume-specific form and considering unary species:

$$p = -\psi^f + \mu C^f; \quad \Pi = -\psi^e + \mu C^e. \tag{5.26}$$

Equation (5.25) can be retrieved by summing the two.

6. Conclusion

This paper presents a novel poromechanical theory for soft nanoporous materials exhibiting two-way coupled sorption–deformation behaviours. The system is treated as a three-phase mixture consisting of solid skeleton, free bulk fluid and sorbed excess phases. Following the Coussy procedure, we develop the admissible forms of generalized transport laws, reaction (sorption) kinetics and constitutive laws of individual phases. Under this framework, we construct a simple effective stress-based model and a general poroelasticity model to capture the complex sorption–deformation patterns of AC interacting with water vapour. The main conclusions are summarized below:

1. By treating the sorptive porous medium as a three-phase mixture, we show that the disjoining pressure is generated by the excess mass sorbed within the pore space. Consequently, the equivalent pore pressure is the summation of the bulk fluid pressure (as measured in a reservoir in equilibrium with the pore) and the disjoining pressure arising from the excess phase.
2. Both the disjoining pressure isotherm and the sorption isotherm originate from the same excess free energy potential—the former as the conjugate to the density variations and the latter to concentration variations of the excess phase. Consequently, they are governed by the same set of parameters.
3. The three-phase formulation provides the flexibility to independently define the constitutive equations of the solid skeleton, the EOS of the bulk fluid and the sorption isotherm of the excess phase. The complex, nonlinear coupling between sorption and deformation emerges organically from the free energy balance of the entire mixture.
4. An equivalent two-phase representation achieved by lumping the bulk and excess phases into a single pore fluid phase is theoretically possible. It may come at the expense of physical clarity and mathematical simplicity offered by the three-phase formulation.

Downloaded from http://royalsocietypublishing.org/rspa/article-pdf/doi/10.1098/rspa.2025.1094/6136174/rspa.2025.1094.pdf
by guest
on 07 May 2026

5. The effective stress-based model with the incompressible solid assumption appears to be robust and efficient for describing the response of cellulose networks interacting with water vapour.
6. The proposed poromechanics theory is consistent with the chemomechanics theory of Gurtin *et al.* [9] and the gel mechanics of Hong *et al.* [11]. The former can be arrived at by removing porosity in the formulation, while the latter is a special case assuming a unary and incompressible fluid.

For the benefits discussed above, the proposed thermodynamic framework offers exceptional flexibility and modularity, making it well-suited to construct a wide range of constitutive models for diverse solid–fluid systems. In particular, the three-phase formulation allows the sorbed excess and bulk fluid phases to possess distinct properties including velocity, pressure, composition and EOS. This allows the different mobilities of nanoconfined, structurally ordered fluid and free bulk fluid to be more accurately represented. Disjoining pressure, a fundamental concept in surface science and colloid research, naturally arises as a property of the excess phase, serving as a bridge that connects research insights across different scales and disciplines. Moreover, the option of having different compositions for the excess and bulk fluid phases makes it possible to capture the varying affinities of different invading species towards the solid skeleton. This capability is particularly important for selective filtration and sorption applications in membrane engineering and sensor technologies. The formulation is sufficiently versatile to extend beyond elastic polymeric materials, encompassing other nanoporous materials that exhibit diverse microstructures and solid–fluid interactions. For example, one promising direction is to apply the theory to describe swelling clays, which contain primarily nanoscale slit pores, have mineral surfaces with a strong affinity for water and exhibit both large deformation and inelastic behaviour.

Data availability. This is a theoretical work with no new data produced. The MD-GCMC data for amorphous cellulose used in this paper are available at Chen *et al.* [2].

Additional derivations are provided in the electronic supplementary material [70].

Declaration of AI use. We have not used AI-assisted technologies in creating this article.

Authors' contributions. Y.Z.: conceptualization, formal analysis, funding acquisition, investigation, methodology, project administration, validation, visualization, writing—original draft, writing—review and editing; I.L.: methodology, writing—review and editing.

Both authors gave final approval for publication and agreed to be held accountable for the work performed therein.

Conflict of interest declaration. We declare we have no competing interests.

Funding. Y.Z. wishes to acknowledge the support of U.S. National Science Foundation under award nos. 2113474 and 2237332 and U.S. Department of Energy under award no. DE-SC0024391.

References

1. Vandamme M. 2019 Coupling between adsorption and mechanics (and vice versa). *Curr. Opin. Chem. Eng.* **24**, 12–18. (doi:10.1016/j.coche.2018.12.005)
2. Chen M, Coasne B, Derome D, Carmeliet J. 2020 Coupling of sorption and deformation in soft nanoporous polymers: molecular simulation and poromechanics. *J. Mech. Phys. Solids* **137**, 103830. (doi:10.1016/j.jmps.2019.103830)
3. Elbaum R, Abraham Y. 2014 Insights into the microstructures of hygroscopic movement in plant seed dispersal. *Plant Sci.* **223**, 124–133. (doi:10.1016/j.plantsci.2014.03.014)
4. Zhao Q, Dunlop JW, Qiu X, Huang F, Zhang Z, Heyda J, Dzubiella J, Antonietti M, Yuan J. 2014 An instant multi-responsive porous polymer actuator driven by solvent molecule sorption. *Nat. Commun.* **5**, 4293. (doi:10.1038/ncomms5293)
5. Ma M, Guo L, Anderson DG, Langer R. 2013 Bio-inspired polymer composite actuator and generator driven by water gradients. *Science* **339**, 186–189. (doi:10.1126/science.1230262)
6. Reyssat E, Mahadevan L. 2009 Hygromorphs: from pine cones to biomimetic bilayers. *J. R. Soc. Interface* **6**, 951–957. (doi:10.1098/rsif.2009.0184)

Downloaded from http://royalsocietypublishing.org/rspa/article-pdf/doi/10.1098/rspa.2025.1094/6136174/rspa.2025.1094.pdf
by guest
on 07 May 2026

7. Lee Y, Kim SK, Park YJ, Cho J, Koo HJ. 2019 A humidity-sensing composite microfiber based on moisture-induced swelling of an agarose polymer matrix. *Polym. Compos.* **40**, 3582–3587. (doi:10.1002/pc.25220)
8. Yang X, Wang W, Miao M. 2018 Moisture-responsive natural fiber coil-structured artificial muscles. *ACS Appl. Mater. Interfaces* **10**, 32256–32264. (doi:10.1021/acsami.8b12144)
9. Gurtin ME, Fried E, Anand L. 2010 *The mechanics and thermodynamics of continua*. Cambridge, UK: Cambridge University Press. (doi:10.1017/CBO9780511762956)
10. Coleman BD, Noll W. 1963 The thermodynamics of elastic materials with heat conduction and viscosity. *Arch. Ration. Mech. Anal.* **13**, 167–178. (doi:10.1007/BF01262690)
11. Hong W, Zhao X, Zhou J, Suo Z. 2008 A theory of coupled diffusion and large deformation in polymeric gels. *J. Mech. Phys. Solids* **56**, 1779–1793. (doi:10.1016/j.jmps.2007.11.010)
12. Flory PJ. 1942 Thermodynamics of high polymer solutions. *J. Chem. Phys.* **10**, 51–61. (doi:10.1063/1.1723621)
13. Brochard L, Vandamme M, Pellenq R-M. 2012 Poromechanics of microporous media. *J. Mech. Phys. Solids* **60**, 606–622. (doi:10.1016/j.jmps.2012.01.001)
14. Dawson C, Vincent JF, Rocca A-M. 1997 How pine cones open. *Nature* **390**, 668–668. (doi:10.1038/37745)
15. Lin S, Xie YM, Li Q, Huang X, Zhou S. 2016 On the shape transformation of cone scales. *Soft Matter* **12**, 9797–9802. (doi:10.1039/C6SM01805J)
16. Biot MA. 1972 Theory of finite deformations of porous solids. *Ind. Univ. Math. J.* **21**, 597–620. (doi:10.1512/iumj.1972.21.21048)
17. Coussy O, Dormieux L, Detournay E. 1998 From mixture theory to Biot's approach for porous media. *Int. J. Solids Struct.* **35**, 4619–4635. (doi:10.1016/S0020-7683(98)00087-0)
18. Atkin R, Craine R. 1976 Continuum theories of mixtures: basic theory and historical development. *Q J Mech Appl Math* **29**, 209–244. (doi:10.1093/qjmam/29.2.209)
19. de Boer T. 1996 Highlights in the historical development of the porous media theory: toward a consistent macroscopic theory. *Appl. Mech. Rev.* **49**, 201–262. (doi:10.1115/1.3101926)
20. Coussy O. 2010 *Mechanics and physics of porous solids*. Chichester, West Sussex, UK: John Wiley & Sons. (doi:10.1002/9780470710388)
21. El Tabbal G, Dangla P, Vandamme M, Bottoni M, Granet S. 2020 Modelling the drying shrinkage of porous materials by considering both capillary and adsorption effects. *J. Mech. Phys. Solids* **142**, 104016. (doi:10.1016/j.jmps.2020.104016)
22. Leng J, Dangla P, Vandamme M. 2025 Modeling of sorption-induced deformations of porous materials due to surface adsorption, capillary effects, and cavitation. *Int. J. Solids Struct.* **327**, 113808. (doi:10.1016/j.ijsolstr.2025.113808)
23. Weissmüller J, Duan H-L, Farkas D. 2010 Deformation of solids with nanoscale pores by the action of capillary forces. *Acta Mater.* **58**, 1–13. (doi:10.1016/j.actamat.2009.08.008)
24. Gor GY, Huber P, Weissmüller J. 2018 Elastocapillarity in nanopores: Sorption strain from the actions of surface tension and surface stress. *Phys. Rev. Mater.* **2**, 086002. (doi:10.1103/PhysRevMaterials.2.086002)
25. Sharma P, Ganti S, Bhate N. 2003 Effect of surfaces on the size-dependent elastic state of nano-inhomogeneities. *Appl. Phys. Lett.* **82**, 535–537. (doi:10.1063/1.1539929)
26. Zhang Y. 2018 Mechanics of adsorption-deformation coupling in porous media. *J. Mech. Phys. Solids* **114**, 31–54. (doi:10.1016/j.jmps.2018.02.009)
27. Eskandari-Ghadi M, Zhang Y. 2021 Mechanics of shrinkage-swelling transition of microporous materials at the initial stage of adsorption. *Int. J. Solids Struct.* **222**, 111041. (doi:10.1016/j.ijsolstr.2021.111041)
28. Eskandari-Ghadi M, Zhang Y. 2022 Effect of pore size distribution on sorption-induced deformation of porous materials: a theoretical study. *Int. J. Solids Struct.* **242**, 111533. (doi:10.1016/j.ijsolstr.2022.111533)
29. Behboodi M, Zhang Y. 2025 Interfacial evolution explains the complex swelling-shrinkage responses of porous materials from vacuum-dry to full liquid saturation. *J. Mech. Phys. Solids* **207**, 106425. (doi:10.1016/j.jmps.2025.106425)
30. Zhou X, Liu S, Zhang Y. 2021 Permeability evolution of fractured sorptive geomaterials: a theoretical study on coalbed methane reservoir. *Rock Mech. Rock Eng.* **54**, 3507–3525. (doi:10.1007/s00603-021-02404-3)
31. Behboodi M, Eskandari-Ghadi M, Xia W, Zhang Y. 2025 An analytical model for the bending and reaction force of hygroscopic bilayers upon water adsorption. *Int. J. Solids Struct.* **309**, 113191. (doi:10.1016/j.ijsolstr.2024.113191)

Downloaded from http://royalsocietypublishing.org/rspa/article-pdf/doi/10.1098/rspa.2025.1094/6136174/rspa.2025.1094.pdf
by guest
on 07 May 2026

32. Sun C, Zhou R, Zhao Z, Bai B. 2020 Nanoconfined fluids: what can we expect from them? *J Phys Chem Lett* **11**, 4678–4692. (doi:10.1021/acs.jpclett.0c00591)
33. Munoz-Santiburcio D, Marx D. 2021 Confinement-controlled aqueous chemistry within nanometric slit pores: focus review. *Chem. Rev.* **121**, 6293–6320. (doi:10.1021/acs.chemrev.0c01292)
34. Huber P. 2015 Soft matter in hard confinement: phase transition thermodynamics, structure, texture, diffusion and flow in nanoporous media. *J. Phys.: Condens. Matter* **27**, 103102. (doi:10.1088/0953-8984/27/10/103102)
35. DeHoff R. 2006 *Thermodynamics in materials science*. Boca Raton, FL: CRC Press.
36. de Feijter JA. 1988 Thermodynamics of thin liquid films. In *Thin liquid films* (ed. IB Ivanov), pp. 1. Marcel Dekker. (doi:10.1201/9780203735732-1)
37. Sircar S. 2019 The genius of Gibbsian surface excess (GSE) framework for fluid (gas or liquid)–Solid adsorption: a powerful practical tool. *Sep. Purif. Technol.* **213**, 235–245. (doi:10.1016/j.seppur.2018.11.070)
38. Sendner C, Horinek D, Bocquet L, Netz RR. 2009 Interfacial water at hydrophobic and hydrophilic surfaces: slip, viscosity, and diffusion. *Langmuir* **25**, 10 768–10 781. (doi:10.1021/la901314b)
39. Chen L, Wu Z, Xu L, Li Z, Zhang Y, Xia W. 2025 Hydration-driven interfacial behaviors of nanoconfined sodium montmorillonite. *Langmuir* **41**, 31 471–31 480. (doi:10.1021/acs.langmuir.5c04534)
40. Füredi M *et al.* 2025 Disentangling adsorption and absorption in microporous polymers. *Small Methods* **9**, e00845. (doi:10.1002/smtd.202500845)
41. Milischuk AA, Ladanyi BM. 2011 Structure and dynamics of water confined in silica nanopores. *J. Chem. Phys.* **135**, 174709. (doi:10.1063/1.3657408)
42. Coussy O. 2004 *Poromechanics*. Chichester: John Wiley & Sons, Ltd. (doi:10.1002/0470092718)
43. Holzapfel GA. 2000 *Nonlinear solid mechanics—a continuum approach for engineering*. Chichester, West Sussex, UK: John Wiley & Sons.
44. de Boer R. 2006 *Trends in continuum mechanics of porous media*. Springer Science & Business Media. (doi:10.1007/1-4020-3144-0)
45. Bhatia SK, Bonilla MR, Nicholson D. 2011 Molecular transport in nanopores: a theoretical perspective. *Phys. Chem. Chem. Phys.* **13**, 15 350–15 383. (doi:10.1039/c1cp21166h)
46. Derjaguin B, Kusakov M. 1936 The properties of thin layers of liquids. *Proc. Acad. Sci. USSR Chem. Series* **5**, 741–753.
47. Gor GY, Huber P, Bernstein N. 2017 Adsorption-induced deformation of nanoporous materials—a review. *Appl. Phys. Rev.* **4**, 011303. (doi:10.1063/1.4975001)
48. Israelachvili JN. 2011 *Intermolecular and surface forces*. New York: Academic Press.
49. Bhatt D, Newman J, Radke C. 2002 Molecular simulation of disjoining-pressure isotherms for free liquid, Lennard-Jones thin films. *J. Phys. Chem. B* **106**, 6529–6537. (doi:10.1021/jp0202136)
50. Eskandari-Ghadi M. 2022 Effect of surface forces on the mechanics of sorption-deformation in microporous media and environment-assisted crack growth in brittle solids. Doctoral dissertation, University of Colorado, Boulder.
51. Gor GY, Paris O, Prass J, Russo PA, Ribeiro Carrott MML, Neimark AV. 2013 Adsorption of n-pentane on mesoporous silica and adsorbent deformation. *Langmuir* **29**, 8601–8608. (doi:10.1021/la401513n)
52. Rudnicki JW. 2014 *Fundamentals of continuum mechanics*. Chichester, West Sussex, UK: John Wiley & Sons.
53. Bertrand T, Peixinho J, Mukhopadhyay S, MacMinn CW. 2016 Dynamics of swelling and drying in a spherical gel. *Phys. Rev. Appl.* **6**, 064010. (doi:10.1103/PhysRevApplied.6.064010)
54. Carr R, Comer J, Ginsberg MD, Aksimentiev A. 2011 Microscopic perspective on the adsorption isotherm of a heterogeneous surface. *J. Phys. Chem. Lett.* **2**, 1804–1807. (doi:10.1021/jz200749d)
55. Brunauer S, Deming LS, Deming WE, Teller E. 1940 On a theory of the van der Waals adsorption of gases. *J. Am. Chem. Soc.* **62**, 1723–1732. (doi:10.1021/ja01864a025)
56. Brunauer S, Emmett PH, Teller E. 1938 Adsorption of gases in multimolecular layers. *J. Am. Chem. Soc.* **60**, 309–319. (doi:10.1021/ja01269a023)
57. Timmermann EO. 2003 Multilayer sorption parameters: BET or GAB values? *Colloids Surf. A* **220**, 235–260. (doi:10.1016/S0927-7757(03)00059-1)
58. Zhang J, Zhao X, Suo Z, Jiang H. 2009 A finite element method for transient analysis of concurrent large deformation and mass transport in gels. *J. Appl. Phys.* **105**, 093522. (doi:10.1063/1.3106628)

Downloaded from http://royalsocietypublishing.org/rspa/article-pdf/doi/10.1098/rspa.2025.1094/6136174/rspa.2025.1094.pdf
by guest
on 07 May 2026

59. Chester SA, Di Leo CV, Anand L. 2015 A finite element implementation of a coupled diffusion-deformation theory for elastomeric gels. *Int. J. Solids Struct.* **52**, 1–18. (doi:10.1016/j.ijsolstr.2014.08.015)
60. Dortdivanlioglu B, Linder C. 2019 Diffusion-driven swelling-induced instabilities of hydrogels. *J. Mech. Phys. Solids* **125**, 38–52. (doi:10.1016/j.jmps.2018.12.010)
61. Vuong A-T, Yoshihara L, Wall W. 2015 A general approach for modeling interacting flow through porous media under finite deformations. *Comp. Methods Appl. Mech. Eng.* **283**, 1240–1259. (doi:10.1016/j.cma.2014.08.018)
62. Bardet J, Choucair W. 1991 A linearized integration technique for incremental constitutive equations. *Int. J. Numer. Anal. Methods Geomech.* **15**, 1–19. (doi:10.1002/nag.1610150102)
63. Chen M, Coasne B, Guyer R, Derome D, Carmeliet J. 2018 Role of hydrogen bonding in hysteresis observed in sorption-induced swelling of soft nanoporous polymers. *Nat. Commun.* **9**, 1–7. (doi:10.1038/s41467-018-05897-9)
64. Chen M, Coasne B, Guyer R, Derome D, Carmeliet J. 2020 A poromechanical model for sorption hysteresis in nanoporous polymers. *J. Phys. Chem. B* **124**, 8690–8703. (doi:10.1021/acs.jpcb.0c04477)
65. Truesdell C. 1984 *Rational thermodynamics*, 2nd edn. New York, NY: Springer-Verlag.
66. de Groot SR, Mazur P. 1962 *Non-equilibrium thermodynamics*. Amsterdam: North-Holland.
67. Hassanizadeh M, Gray WG. 1980 General conservation equations for multi-phase systems: 3. Constitutive theory for porous media flow. *Adv. Water Res.* **3**, 25–40. (doi:10.1016/0309-1708(80)90016-0)
68. Biot MA. 1956 Theory of propagation of elastic waves in a fluid-saturated porous solid. I. Low-frequency range. *J. Acoust. Soc. Am.* **28**, 168–178. (doi:10.1121/1.1908239)
69. Anand L. 2015 2014 Drucker medal paper: a derivation of the theory of linear poroelasticity from chemoelasticity. *J. Appl. Mech.* **82**, 111005. (doi:10.1115/1.4031049)
70. Zhang Y, Lunati I. 2026 Supplementary Material: Sorption-deformation coupling in soft nanoporous materials: insights from a three-phase poromechanics theory. Figshare. (doi:10.6084/m9.figshare.c.8407467)

Downloaded from http://royalsocietypublishing.org/rspa/article-pdf/doi/10.1098/rspa.2025.1094/6136174/rspa.2025.1094.pdf
by guest
on 07 May 2026